Journal of the Mechanical Behavior of Biomedical Materials 91 (2019) 76–90

Contents lists available at ScienceDirect

Journal of the Mechanical Behavior of Biomedical Materials

journal homepage: www.elsevier.com/locate/jmbbm

A shear assay study of single normal/breast cancer cell deformation and detachment from poly-di-methyl-siloxane (PDMS) surfaces

C.J. Ani[a,b], J.D. Obayemi[c], V.O. Uzonwanne[c], Y. Danyuo[d,e], O.S. Odusanya[f], J. Hu[g], K. Malatesta[g], W.O. Soboyejo[c,e,f,*]

[a] Department of Theoretical and Applied Physics, African University of Science and Technology, Km 10, Airport Road, Galadimawa, Abuja, Federal Capital Territory, Nigeria
[b] Department of Physics, Salem University, Km 16, PMB 1060, Lokoja, Kogi State, Nigeria
[c] Department of Mechanical Engineering, Worcester Polytechnic Institute (WPI), Worcester, MA 01609, USA
[d] Department of Mechanical Engineering, Ashesi University, Berekuso, Ghana
[e] Department of Materials Science and Engineering, African University of Science and Technology, Km 10, Airport Road, Galadimawa, Abuja, Federal Capital Territory, Nigeria
[f] Advanced Biotechnology Laboratory, Sheda Science and Technology Complex, Abuja, Nigeria
[g] Princeton Institute for the Science and Technology of Materials (PRISM), and The Department of Mechanical and Aerospace Engineering, Princeton University, Princeton, NJ 08544, USA

ARTICLE INFO

Keywords:
Cell deformation and detachment
Shear assay technique
Viscoelastic cell deformation
Vinculin pull-out
Interfacial fracture

ABSTRACT

This paper presents the results of a combined experimental and analytical/computational study of viscoelastic cell deformation and detachment from poly-di-methyl-siloxane (PDMS) surfaces. Fluid mechanics and fracture mechanics concepts are used to model the detachment of biological cells observed under shear assay conditions. The analytical and computational models are used to compute crack driving forces, which are then related to crack extension during the detachment of normal breast cells and breast cancer cells from PDMS surfaces that are relevant to biomedical implants. The interactions between cells and the extracellular matrix, or the extracellular matrix and the PDMS substrate, are then characterized using force microscopy measurements of the pull-off forces that are used to determine the adhesion energies. Finally, fluorescence microscopy staining of the cytosketelal structures (actin, micro-tubulin and cyto-keratin), transmembrane proteins (vimentin) and the ECM structures (Arginin Glycine Aspartate – RGD) is used to show that the detachment of cells during the shear assay experiments occurs via interfacial cracking between (between the ECM and the cell membranes) with a high incidence of crack bridging by transmembrane vinculin structures that undergo pull-out until they detach from the actin cytoskeletal structure. The implications of the results are discussed for the design of interfaces that are relevant to implantable biomedical devices and normal/cancer tissue.

1. Introduction

The deformation and detachment of biological cells from the extracellular matrix materials between biological cells and the substrates are crucial to cell function (Yoon and Mofrad, 2011). They also play an important role in tissue regeneration around biomedical implants (Maxwell et al., 2005) and Bio-Micro-Electro-Mechanical Systems (BioMEMS) (Bashir, 2004) that are relevant to orthopaedics and dentistry (Fu et al., 2009) and cardiovascular diseases (Curtis and Russell, 2009; Prat-vidal et al., 2013).

The deformation and detachment processes are mediated by complex bimolecular proteins that are over-expressed on the surfaces of cells and extracellular matrices. The cell/surface receptor proteins bind specifically to the ligand proteins (Hynes, 2002). The clustered receptor-ligand bound and cytoskeletal proteins form focal contacts or focal adhesions that anchor the cells to the surfaces (Izzard and Lochner, 1976).

Cell deformation and detachment depend largely on the mechanical properties of the cell (Liu and Wang, 2004; Engler et al., 2009; Hong-Lian et al., 2004). These are determined by its intracellular components (cytoskeleton, nucleus, cytosol and several other organelles) and the interactions of the cell membrane/receptors with extracellular microenvironments and the substrate (Peeters et al., 2005). Prior experimental work has also shown that the differences in the mechanical

* Correspondence to: Department of Mechanical Engineering, Worcester Polytechnic Institute, Olden Street, Worcester, MA 01609, USA.
E-mail address: wsoboyejo@wpi.edu (W.O. Soboyejo).

https://doi.org/10.1016/j.jmbbm.2018.11.012
Received 8 May 2015; Received in revised form 25 June 2018; Accepted 12 November 2018
Available online 15 November 2018
1751-6161/ © 2018 Elsevier Ltd. All rights reserved.

properties of cells are correlated with pathophysiological states in many diseases, such as cancer (Cross et al., 2007; Lekka et al., 1999; Kuznetsova et al., 2007; Guo et al., 2012; Suresh, 2007), malaria (Lee and Lim, 2007), diabetes (Lee and Lim, 2007) and sickle cell anemia (Williamson et al., 1985).

The cytoskeleton network and its components primarily determine the cell's shape and mechanical deformation characteristics (Suresh, 2007). Abnormal cellular functions can also change the cytoskeletal structures resulting in significant variations in mechanical properties (Suresh et al., 2005). Prior work (Cross et al., 2007; Lekka et al., 1999) has shown that the Young's moduli of breast cancer cells are significantly lower than those of healthy cells (Fuhrmann et al., 2011; Xu et al., 2012a, 2012b; Suresh, 2007). Such lowering of Young's moduli has also been shown to result in the increased compliance or deformability of cancer cells, compared to those of normal cells. This is partly attributed to the up- or down-regulation of cyto-skeletal structures (Efremov et al., 2015) and adhesion proteins (Xu et al., 2012a) that can affect cell shape and the binding to normal cells and cancer cells to different substrates.

Accompanying the changes in cellular mechanical properties are some very specific changes in the extracellular environment (Erler et al., 2006). This includes the remodeling of the collagen fibers within the ECM (Stein et al., 2011). Such remodeling can occur due to strain-induced stretching that alters the structure and the mechanical properties of the ECM (Stein et al., 2011).

Furthermore, the mechanical properties of the cell nucleus are also important for the mechano-transduction pathways (Li and Lim, 2010; Isermann and Lammerding, 2013). Such mechano-transduction pathways can give rise to changes (mutation) in the nuclear structure which can cause impaired nuclear mechanics (Zwerger, Ho, and Lammerding, 2011). This suggests that differences in cell mechanical properties may provide important clues for the early detection of cancer (Xu et al., 2012a, 2012b).

Also, due to the importance of the adhesive interactions between biological cells and surfaces, a number of researchers (Evans, 1980; Tözeren et al., 1992; Moy et al., 1999) have developed experimental techniques for the measurement of cell elastic/viscoelastic properties and cell detachment forces. Evans (Evans, 1980) has explored the micropipette manipulation method for the measurement of adhesion energies of red blood cells. This was accomplished by monitoring the reduction of the aspirated "tongue" in the pipette, upon adhesion. Tözeren et al. (1992) has also used micropipette aspiration to measure the detachment of T-type lymphocytes from a planar membrane that contains ICAM-1 ligand molecules.

Furthermore, Moy et al. (1999) have measured the free energies associated with the separation of two bioactive surfaces in contact. This was modeled using a cell-free thermodynamics approach, based on the Johnson-Kendal-Roberts (JKR) model (Moy et al., 1999). The model was used to examine the role of the binding affinity of ligand-receptor complexes in surface adhesion. Prechtel et al. (2002) also proposed a method that is based on micropipette manipulation. This was used to study the dissociation of adhesive contacts between living cells and ligand-decorated vesicles subjected to a linear ramp force. Yield forces at the rim (which are dimensionally equivalent to energy densities), were found to scale as a power of the loading rate.

Several computational models (Yamamoto et al., 1998; Fu et al., 2009) have been used to study the effects of cell mechanical properties on the deformation and detachment of biological cells from biomaterials surfaces. Gaver and Kute (Gaver and Kute, 1998) computed the mechanical stress, fluid drag on two-and three-dimensional rigid semi-circle adherent cell on the wall of a micro-channel. They showed that the fluid drag increased with decreasing chamber size. The fluid drag was also shown to decrease with decreasing chamber size, as the assumed semi-circular "rib-shaped" cell and cell height decrease.

The rolling adhesion of deformable leukocytes has been considered in two-dimensions by Dong et al. (Dong et al., 1999; Dong and Lei, 2000; Lei, Lawrence, and Dong, 1999). They modeled leukocytes as viscous liquid droplets surrounded by an elastic ring. They showed that the fluid drag on adherent leukocytes decreased with increasing cell deformation and microchannel size. Liu and Wang (2004) also studied the deformation of an adherent leukocyte and the forces exerted on it. The distribution of pressure on the cell membrane confirmed the existence of a high-pressure region, downstream of the drop. This retarded further deformation of the cell and provided a positive lift force on the drop.

Furthermore, the considerations of the relatively high viscosity of the nucleus can help to correct for the over-estimation of cell deformation within a flow field. Also, adherent leukocytes exposed to a shear flow, undergo deformation that increases with the initial contact angle, the capillary number, and the Reynolds number (Liu and Wang, 2004). However, this deformation has a limit (Rinko, Lawrence, and Guilford, 2004; Fu et al., 2009). The detachment forces exerted on the cell also depend largely on the cell's shape (Xiao and Truskey, 1996; Fu et al., 2009).

Nevertheless, although the basic understanding of cell deformation and mechano-transduction phenomena has increased in recent years (Lei et al., 1999; Liu and Wang, 2004), there is still only a limited understanding of the cell deformation and interfacial fracture phenomena associated with shear assay conditions (Liu and Wang, 2004) that are relevant to biomedical implants (Weisenberg and Mooradian, 2002), BioMEMS, and bio-electronics.

This paper presents the results of a combined experimental and computational fluid dynamics (CFD)/computational linear elastic fracture mechanics (CLEFM) study of shear assay measurements of cell detachment from PDMS (a model substrate material that is used in BioMEMs and bioelectronics applications). The models are used to compute the detachment conditions for single breast cancer cells and normal breast cells from biocompatible uncoated poly-di-methyl-siloxane (PDMS) surfaces. A combination of analytical and computational models is also used to study cell deformation and the detachment of normal breast cells/breast cancer cells from PDMS. The implications of the results are then discussed for the design of implantable biomedical devices.

2. Experimental methods

2.1. Cell culture

Prior to the extraction of the secreted Extra-Cellular Matrix (ECM) via the shear assay method (Fu et al., 2009), the mammary human breast cancer cell line MDA-MB-231 and the non-tumorigenic human mammary epithelial cell line MCF10A were cultured under conditions described in detail in Wong et al. (2015a), (2015b). First, 20 μl of 1×10^5 MDA-MB-231 cells were cultured in 60 × 15 mm and 35 mm Falcon Petri dishes (Falcon, Franklin Lakes, NJ, USA) at 37 °C. This was done using an L-15 medium (ATCC, Manassas, VA, USA), supplemented with 100 I.U./ml penicillin/100 g/ml streptomycin and 10% FBS (ATCC, Manassas, VA, USA) ($L15^+$ medium).

The MCF 10A cells were grown under cell culture conditions described by (Wong et al., 2015a, 2015b; Cailleau et al., 1974). 20 μl of 1×10^5 of MCF10A cells were cultured at 37°C in 5% CO2 in the following medium: DMEM/F12 medium (Invitrogen # 11330-032) supplemented with 5% horse serum (Invitrogen# 16050-122), 30 ng/ml murine Epidermal Growth Factor (Peprotech #315-09), 0.5 lg/ml hydrocortisone (Sigma Aldrich), 100 ng/ml cholera toxin (Sigma Aldrich), 10 lg/ml insulin (Sigma #I-882-100MG), 1% Penicillin-Streptomycin (ATCC # or Invitrogen #15070-063), and 0.2% amphotericin (Gemini Bioproducts, #400-104).

2.2. Extraction of ECM using the shear assay technique

MCF 10A cells and MDA MB 231cells were cultured in 35 mm

Falcon dishes (Corning Inc., Corning, NY, USA) for 48 h. This was done to ensure that the trans-membrane and extra-cellular matrix proteins were secreted and self-organized. Furthermore, in an effort to harvest the extra-cellular matrix secreted by MDA MB 231 cells and MCF 10A, a shear assay technique was used to shear off the cells, after culturing for 72 h to secrete the ECM. The technique, which uses a laminar shear flow (of cell culture fluid) to shear off biological cells, can also be used to reveal the underlying ECM that is left behind after the shear detachment of the biological cell (Fu et al., 2009).

In the current work, a parallel plate flow chamber (Glycotech Corporation, Rockville, Maryland, USA) with a width of 2.5 mm, height of 0.25 mm and length of 34 mm was used. The cell culture fluid was pumped through Tygon tubing into the shear assay chamber. The deformation and detachment of the cells was also observed using an inverted microscope (Nikon Instruments, Melville, NY, USA) equipped with a bright field camera (Lumenera Corporation, Ottawa, ON, Canada). The flow rates of the cell culture fluid were increased until the cells started detaching under in-situ observation.

2.3. Adhesion measurements

After cell detachment, the cell samples were rinsed with sterile Dulbecco phosphate buffered saline (DPBS; Invitrogen, Carlsbad, CA) and fixed with 1.5 ml of paraformaldehyde 4% in 0.1 M phosphate buffer saline (Sigma-Aldrich, St. Louis, MO, USA) for 10 min at a room temperature. The fixed cells were further rinsed with DPBS, followed by a final rinse with deionized water. Finally, the cell samples were placed in a vacuum desiccator for 3 h to dry at room temperature (25℃).

The secreted ECM on petri dishes left behind by the detached cell lines (during the shear assay experiments) were observed using an inverted microscope (Nikon Instruments, Melville, NY, USA). The ECM from the two cell lines were dip-coated onto AFM tips that were procured from Sigma-Aldrich, St. Louis, MO, USA. The coated AFM tips were then air-dried for about 5 min.

The resulting coated AFM tips were then used in force microscopy experiments that measured the adhesion forces between the coated AFM tips and the breast cancer cells (MDA-MB 231 cells) or normal breast cells (MCF 10A cells). Adhesion was measured using a Multimode Dimension DI Nanoscope IIIa Atomic Force Microscope (Bruker Instruments, Woodbury, NY, USA).

Prior to adhesion measurement, the spring constants of the coated AFM tips were measured experimentally using the thermal tune method (Hutter and Bechhoefer, 1993; Matei et al., 2006; Hampp et al., 2012). This was done to obtain the actual spring constants that were used to calculate the pull-off forces. The thermal tune measurements of the spring constants were needed to account for the batch-to-batch variations in the spring constants, as well as the effects of extracellular matrix (ECM) coatings on the stiffnesses of the AFM cantilevers.

Force microscopy experiments were carried out using a Dimension 3100 AFM (Bruker Corporation, Billerica, MA, USA). The experiments were performed at room-temperature (22 ˚C) and a relative humidity of 36–45%. Before each adhesion force measurement, the photodetector sensitivity was calibrated using a stiff quartz platform (Bhushan, 1999; Wolf et al., 2008).

The adhesion forces were then measured between AFM tips that were dip-coated with healthy/normal ECM or cancerous ECM and normal breast cells (MCF-10A cells) or breast cancer cells (MDA-MB-231 cells). For each pair of adhesive interactions, 6 adhesion measurements were obtained from two AFM tips, with each AFM tip being used for 3 measurements.

2.4. Immunofluorescence microscopy

2.4.1. Cytoskeleton staining

Immuno-fluorescence (IF) staining was used to reveal the cytoskeletal structures of the MCF-10A normal breast cells and MDA-MB-231 triple negative breast cancer cells. This was used to characterize the distribution and relative densities of F-actin, alpha-tubulin, vimentin and cyto-keratin 8/18 structures. Prior to IF staining, the two cell lines were cultured separately on 1.5 coverslips. This was done in sterile 60 mm × 15 mm Petri dishes in their respective media.

After 48 h, the cells were fixed for 10 min with 4% high-grade paraformaldehyde (4% in 0.1 M PBS, Electron Microscopy Science, Hatfield, PA, USA). The paraformaldehyde was then aspirated after fixing. This was followed by three rinses with Phosphate Buffer Solution (PBS). The cell samples were then permeabilized, each with 1 ml 0.1% solution of Triton X-100 (Life Technologies Corporation, Carlsbad, CA, USA) for 10 min. This was again followed by three rinses with PBS.

Subsequently, the cell samples were incubated in PBS with 1% BSA (Sigma-Aldrich, St. Louis, MO, USA) at room temperature (25℃) for 1 h. This was done to block nonspecific binding. The samples were then rinsed thrice with PBS, before labeling with Tubulin alpha Rabbit Polyclonal Antibody (Thermo Fisher Scientific) at 2 μg/ml in 0.1% BSA or Vimentin Mouse Monoclonal Antibody (Thermo Fisher Scientific, Waltham, MA, USA) at 2 μg/ml in 0.1% BSA or cyto-keratin 8 (TS1) Mouse Monoclonal Antibody (Thermo Fisher Scientific, Waltham, MA, USA) at 2 μg/ml in 0.1% BSA.

The labeled structures were then incubated for 3 h at room-temperature (25℃). This was followed by three rinses with PBS prior to labeling for 45 min at 25℃ with Goat anti-Mouse IgG (H + L) Superclonal™ Secondary Antibody, Alexa Fluor® 488 conjugate (Thermo Fisher Scientific, Waltham, MA, USA) at a dilution of 1:2000. This was followed by three rinses with PBS and the incubation of the cells for 25 min. Incubation was carried out in the dark at room-temperature (25℃). The resulting structures were then stained with the F-actin stain Rhodamine Phalloidin (Thermo Fisher Scientific, Waltham, MA, USA) in PBS. This was followed by three rinses with PBS.

Finally, the cell nuclei were stained with SlowFade® Gold Antifade Mountant with DAPI (Thermo Fisher Scientific, Waltham, MA, USA) for 2 min. The resulting samples are then mounted on clean glass slides, with a drop of Fluoro Guard Reagent (Bio-Rad Laboratories, Hercules, CA, USA) as the mounting medium.

The stained cell samples were imaged using a 60X oil immersion objective, with an inverted Leica SP5 Point Scanning Confocal Microscope (Leica Microsystems, Heidelberg, Germany). Confocal imaging was performed under identical system parameter settings. Quantification of the Corrected Total Cell Fluorescence (CTCF) was obtained for actin, β-tubulin, vimentin and cyto-keratin 8 staining of MCF 10A cell lines and MDA-MB 231 cell lines. This was done using the ImageJ software package (NIH, 2012, Bethesda, Maryland, USA). The CTCF is calculated according to the following formula (Gavet and Pines, 2010):

$$\text{CTCF} = \text{IDP of cell} - (\text{Area of the selected cell x MFB}) \quad (1)$$

where IDP represents the Integrated Density Pixels of the cell and MFB represents the Mean fluorescence of background.

The alteration of the cytoskeletal structures (associated with cancer progression) was also characterized using the Relative Fluorescence (RF), which is given by the ratio of the CTFC of the actin filaments to that of the microtubules or intermediate filaments (i.e., cyto-keratin or vimentin) per cell. This is given by:

$$RF = \frac{CTFC\ of\ the\ Actin Filaments}{CTFC\ for\ tubulins\ or\ intermediate\ filaments} \quad (2)$$

2.4.2. Vinculin/focal adhesion staining after shear assay

Focal adhesion formation is characterized by the attachment of intracellular alpha/beta integrin components to intermediate proteins such as vinculin which in turn are connected to the cytoskeleton through bundles of actin filaments. Thus, in this section, Immunofluorescence staining of vinculin and actin structure after the cells were subjected to shear flow that creates cell-substrate detachment

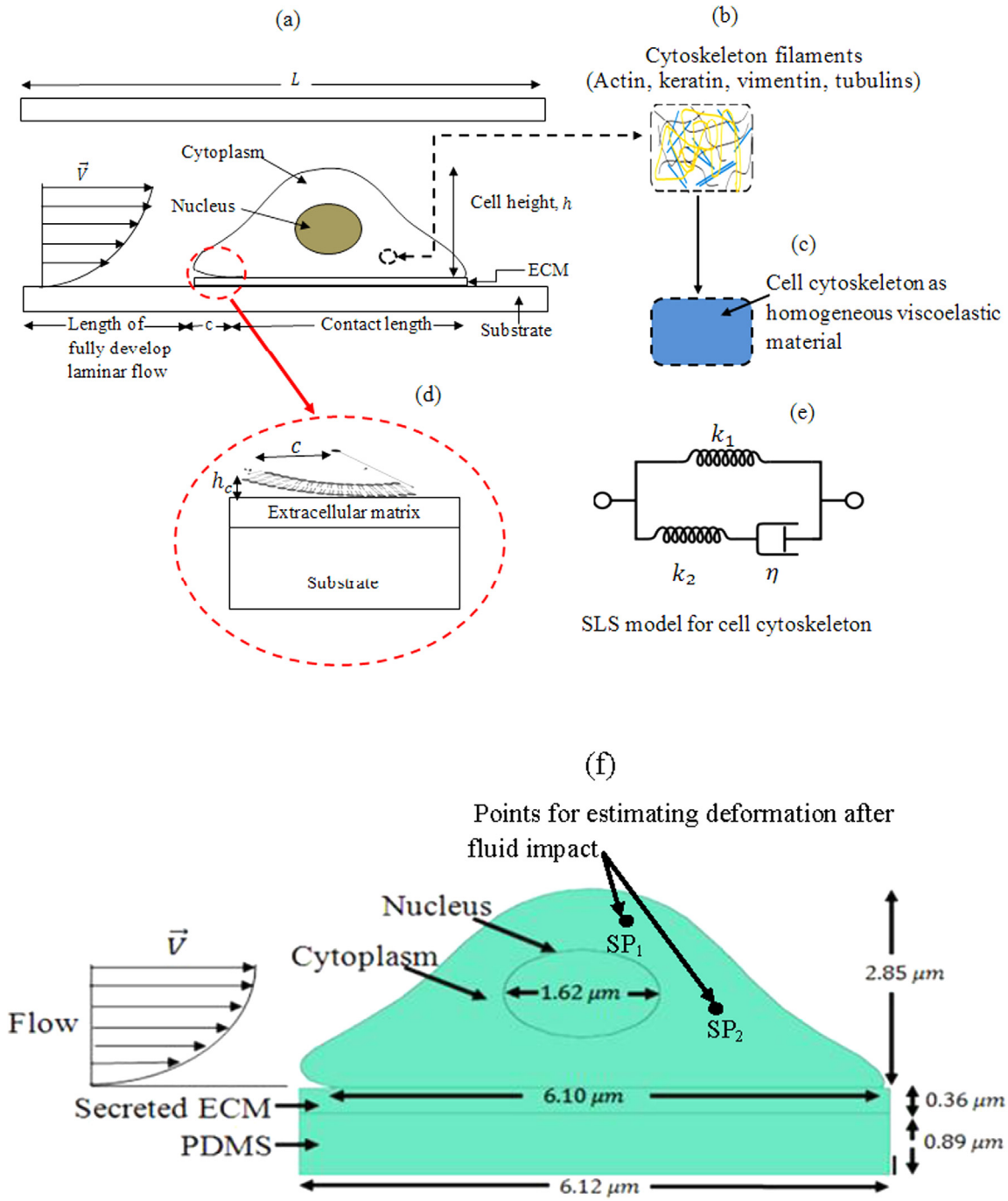

Fig. 1. Schematics of: (a) Cell deformation and detachment model for finite element analysis, (b) Cytoskeleton filaments (actin, keratin, vimentin, tubulins), (c) Cell cytoskeleton as homogeneous viscoelastic material, (d) Standard linear solid model for cytoskeleton.

were performed to reveal the presence of cytoskeletal structures (actin, micro-tubulin, cyto-keratin), transmembrane protein (vinculin) and ECM (RGD) in the initial cells (before detachment) and on the residual materials that were left by the cells on the PDMS substrates after cell detachment. This was done during the 70% confluent log phase on MDA MB 231 cells and MCF10A cells.

First, the cells were fixed with 4% paraformaldehyde for 12 min and rinsed three times with a combination of 10% DPBS and 90% DiH_2O (Washing solvent). The cells were then permeabilized with 0.1% Triton™ X-100 for 10 min and then blocked with 1% BSA for 1 h under room temperature. The BSA-treated ECM were then rinsed three times with the washing solvent before labeled with vinculin Mouse Monoclonal Antibody (Product # MA5-11690, Thermo Fisher Scientific, Waltham, MA, USA) at 2 μg/ml prepared in 0.1% BSA and incubated for 3 h at room temperature. The resulting sample were rinsed three times and then was labeled with Goat anti-Mouse IgG (H + L) Superclonal™ Secondary Antibody, Alexa Fluor® 488 conjugate (Product # A28175, Thermo Fisher Scientific, Waltham, MA, USA) at a dilution of 1:2000 for 45 min at room temperature.

The nuclei were stained with SlowFade® Gold Antifade Mountant with DAPI (Product # S36938, Thermo Fisher Scientific, Waltham, MA, USA), while F-actin was stained with Alexa Fluor® 555 Rhodamine Phalloidin (Product # R415, Thermo Fisher Scientific, Waltham, MA, USA). The images were captured with HCX PL APO CS 40X 1.25 oil objective in Leica SP5 Point Scanning Confocal Microscope.

3. Modeling

Prior shear assay studies have been used to determine the adhesion strengths of HOS cells on selected biomaterial surfaces (Fu et al., 2009). These studies showed that biological cells are not incompressible. They also showed that there is a significant change in the contact area and cell shapes that are observed during shearing (Cao et al., 2007; Bly et al., 2007; Fu et al., 2009). The shear assay studies were used to measure the cell detachment stresses, the interfacial strengths and the viscoelastic properties of the nucleus and the cytoplasm. However, simple viscoelastic models were used, and the cell detachment processes were considered as interfacial failure processes without including the role of cracks.

3.1. Modeling of fluid flow

We assume a fully developed, two-dimensional, steady laminar incompressible fluid flow through the microchannel (without the cell present). At the surfaces of the lower and upper boundaries of the flow channel, and also along the surfaces of the adhered cell, no slip and no penetration conditions were assumed. Also, since the Reynolds number of the flow is very small, $Re=\frac{\rho h U_{ave}}{\mu} \ll 1$, where U_{ave} is average flow velocity, ρ is the fluid density and μ is the viscosity. Fluid motion was assumed to be governed by the continuity and Navier-Stokes equations. These are given, respectively, by Katz (2010):

$$\rho\frac{d\vec{V}}{dt} = -\nabla P + \mu\nabla^2 \vec{V} \tag{3}$$

and

$$\vec{\nabla}\bullet\vec{V} = 0 \tag{4}$$

where ∇P is the pressure gradient and $\vec{V} = (u, v)$ is the convective velocity of the fluid. Furthermore, a no-slip boundary condition was imposed. Hence, the velocities at the top and the bottom walls of the microchannel are zero. These give:

$$\vec{V}(x, y = y_{wall}) = 0 \tag{5}$$

and

$$U_{ave} = \frac{H^2\Delta P}{12\mu L} and\ \tau_w = \frac{H\Delta P}{2L} \tag{6}$$

where L and H are the length and height of the channel, respectively, and μ is the fluid viscosity. For scenarios in which the cell is now present in the microchannel, laminar flow was assumed before fluid impact on the cell's frontal area. An initial cell debonding was assumed to occur over a height h_c above the interfacial membrane opening "c" of cell-ECM interface (Fig. 1a). The shear stress is applied to the cell membrane (up to a height $y = h_c$), as shown in Fig. 1. The shear stress, τ_w, is given by:

$$\tau_{w|y=h_c} = \frac{H\Delta P_b}{2b}\left(1-\frac{2h_c}{H}\right) = \frac{6\mu H}{{h_c}^3}\left(1-\frac{2h_c}{H}\right) \tag{7}$$

where b is the distance covered by the fully developed laminar fluid flow before impact with the cell, ΔP_b is inlet fluid pressure before impact with the cell, h_c is height of cell membrane above the ECM of cell, μ is the fluid viscosity and H is the height of the micro-channel.

3.2. Model of cytoskeleton as fiber reinforced composites

The cytoplasm of a biological cell composed of an organized network of the cytoskeleton of actin microfilaments, intermediate filaments, and microtubules (Spencer, 2011). These three major families of polymers control the shape and mechanics of biological cells. The most important differences that distinguish the three main cytoskeletal polymers are in the architecture and function of the networks they form, their mechanical stiffness, the dynamics of their assembly, their polarity, and the type of molecular motors with which they associate (Fletcher and Mullins, 2010). The spatial organizations of these networks share a mutual interdependence (Weber and Bement, 2002). The disassembly of one network by pharmacological treatments often affects the organization of another (Green and Goldman., 1983; Goldman et al., 1996; Wickstrom et al., 1995).

Several studies have explored the contributions of actin and microtubules to cellular rheology (Korb et al., 2004; Janmaleki et al., 2016; Kubitschke et al., 2017). However, the understanding of the particular role of intermediate filaments to cellular deformation is beginning to emerge (Ramms et al., 2013; Seltmann et al., 2013; Gladilina, Gonzaleza, and Eilsa, 2014). When intermediate filaments organization is disrupted, the actin network is re-organized, whereas microtubule organization remains largely unaltered (McCormick et al., 1993; Esue et al., 2006). Alternatively, the intermediate filaments network collapses, following microtubule disassembly, and re-organizes upon actin depolymerization (Croop and Holtzer, 1975; Cary et al., 1994).

The results from the above studies have stimulated recent studies that have attempted to build computational models of human cells that incorporate various components of cellular substructure and their properties (Barreto et al., 2013; Xue et al., 2015). Although early work focused on the continuum-based/constitutive modeling of cells as homogeneous isotropic materials that contain the cytoplasm and the nuclei, and other components of the cell (Unnikrishnan, Unnikrishnan, and Reddy, 2007; Fallqvist et al., 2016).

More recent studies have tried to explore the contribution of cytoskeletal components, such as actin and vimentin intermediate filaments (Gladilina et al., 2014), to cell deformation. Recent work has shown that these cytoskeletal structures contribute significantly to the viscoelastic deformation of biological cells, which depend on cell-type and disease-state (Nematbakhsh et al., 2017; Schierbaum et al., 2017; Trickey et al., 2004).

Hence, in this study, we explore the contributions of the actin, tubulin, cyto-keratin, and vimentin structures on the deformation and detachment of single adherent healthy and cancerous cells under shear flow conditions. We idealize the cytoplasm as a fiber-reinforced composite and the nucleus as a homogeneous material in a composite.

The cytoplasm is considered as composite with randomly oriented actin filaments in a matrix of microtubules and intermediate filaments as observed in our immunofluorescence experiments on MCF 10A cell lines and MDA-MB 231 cell lines (Figs. 2–4(a,b)). Using such an idealization, the effective properties of the cytoplasm (i.e. matrix of microtubules and intermediate filaments) reinforced with actin filaments could be obtained by using composite theories (Hult and Rammerstorfer, 1994).

Assuming a homogeneous continuum within a representative volume element (RVE), (Fig. 1(b, c)) *containing a large set* of cytoskeletal *filaments*, the "effective" Young's modulus of the homogenized cytoskeleton can be estimated from rule-of-mixture theory. This is given by (Gibson, 1994; Soboyejo, 2002):

$$E_{eff} = \varphi_m E_m(t) + \xi\varphi_f E_f(t) \tag{8}$$

where φ_m is the volume fraction of matrix (of microtubules and intermediate cytoskeletal structure), is the volume fraction actin filaments, $E_m(t)$ is the Young's modulus of the matrix at time, t, and $E_f(t)$ is the Young's modulus of the cytoskeletal actin filaments at time, t (Pachenari et al., 2014; Iversen, 2015). The volume fractions of the nuclei and cytoskeletal filaments in the cell lines obey the law of mass conservation (i.e., $\varphi_m + \varphi_f + \varphi_n = 1$) (Mofrad and Kamm, 2006), and φ_n, $\varphi_f and \varphi_m$ represent the volume fractions of nucleus, actin filaments and matrix of microtubules and intermediate filaments. Also, the orientation factor for actin filaments, ξ, is obtained from Yan and Marriott (2003). The immuno-fluorescence images of MCF 10A cell lines and

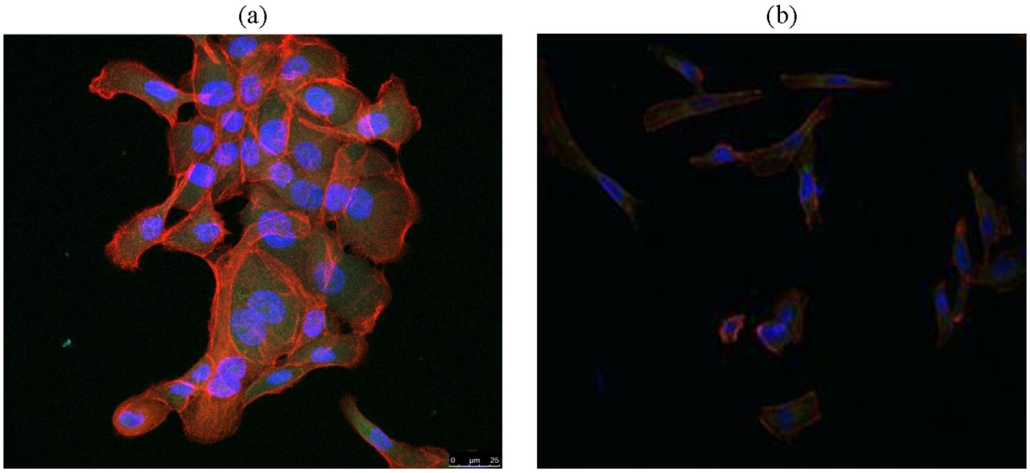

Fig. 2. (a) MCF 10A cells with Actin (Red), Tubulin (Green), and Nucleus (Blue); (b) MDA-MB 231 cells with Actin (Red), Tubulin (Green), and Nucleus (Blue).

MDA-MB 231 cells were analyzed using the ImageJ software package (ImageJ, NIH, Bethesda, MD). This was used to quantify the volume fractions of the cytoskeletal filaments.

3.3. Viscoelastic deformation

Carmichael et al. (2015) have presented the viscoelastic parameters of the cytoskeletal networks in MCF 10A cells and MDA-MB-231 cells. These were incorporated into the current finite element models of the MCF 10A and MDA-MB-231 cells in this study. We also used a standard linear model to account for the viscoelastic responses of cells exposed to shear stresses that are induced during the shear assay experiments. This standard linear model includes an elastic element (modulus k_1). This provides the restoring force that is needed to recover the initial cell shape after the release of the stress. This is arranged in parallel with another elastic element (modulus k_2) in series with a viscous element (μ). The relationship between the relaxation time constant, τ, and the elastic (k_1 and k_2) and viscous (μ) parameters is given by Sato et al. (1996):

$$\tau = \frac{\mu}{k_1}\left(1 + \frac{k_1}{k_2}\right) \tag{9}$$

The viscoelastic properties can be defined with a Prony expansion of the dimensionless shear and bulk relaxation moduli. The Prony expansion of the time-dependent shear behavior is given by (Pettermann and Hüsing, 2012):

$$g_R(t) = 1 - \sum_{i=1}^{N} \bar{g}_i^{\,p}\left(1 - e^{-t/\tau_i^G}\right) \tag{10}$$

where $g_R(t) = G_R(t)/G_0$ is the dimensionless shear relaxation modulus, $G_R(t)$ is the shear modulus at the time t, G_0 is the initial shear modulus, ν is the Poisson's ratio, N is the number of terms in the Prony series, $\bar{g}_i^{\,p}$ is the dimensionless Prony series parameter for the shear modulus, G, and τ_i^G is the relaxation characteristic time. Several studies have used the shear relaxation behavior to characterize the time dependent changes in cell stiffness (Tan et al., 2008; Fisseha and Katiyar, 2012; Sato et al., 1990; Zhou, Lim, and Quek, 2005). Similarly, the time-dependent bulk behavior of the material can be expressed in the form of (Pettermann and Hüsing, 2012):

$$k_R(t) = 1 - \sum_{i=1}^{N} \bar{k}_i^{\,p}\left(1 - e^{-t/\tau_i^K}\right) \tag{11}$$

where $k_R(t)$ is the dimensionless bulk relaxation modulus, τ_i^K is the relaxation characteristic time, and $\bar{k}_i^{\,p}$ is the dimensionless Prony series parameter for the bulk modulus, K. The bulk relaxation behavior reflects the time-dependent changes in cell volumetric behavior. It has recently been included in modeling the cell compression (McGarry,

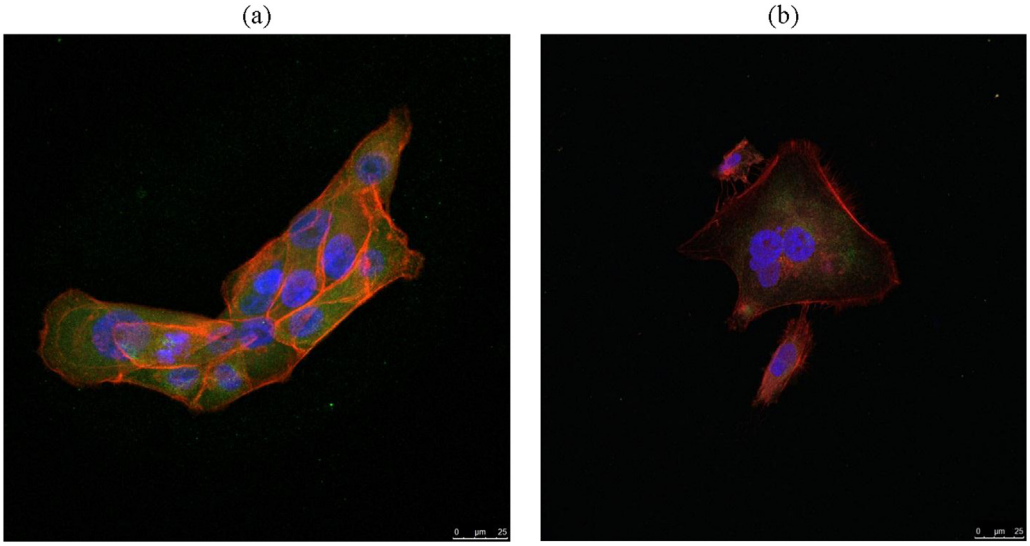

Fig. 3. (a) MCF 10A cells with Actin (Red), Vimentin (Green), and Nucleus (Blue); (b) MDA-MB 231 cells with Actin (Red), Vimentin (Green), and Nucleus (Blue).

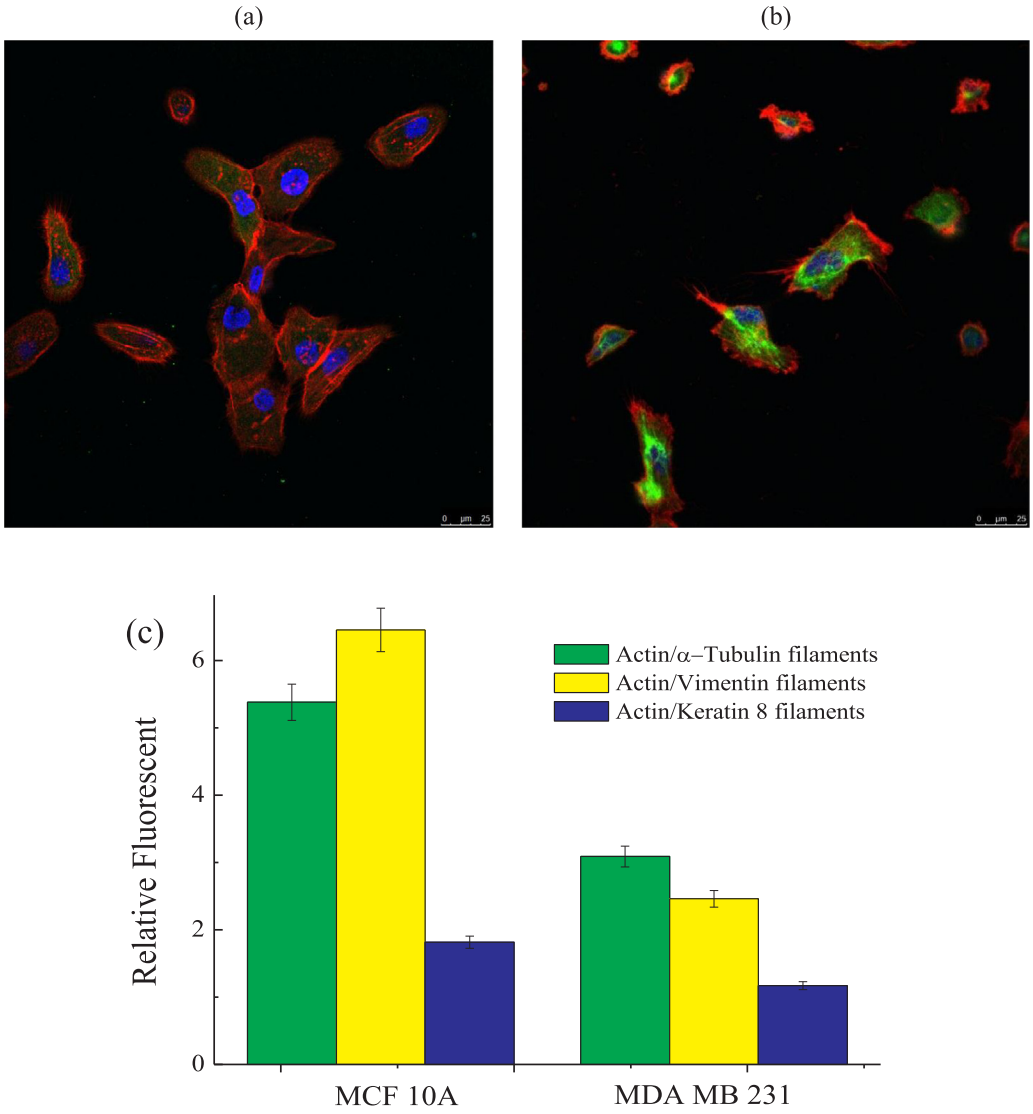

Fig. 4. (a) MCF 10A cells with Actin (Red), Cytokeratin 8 (Green), Nucleus (Blue); (b) MDA-MB 231 cells with Actin (Red), Cytokeratin 8 (Green), Nucleus (Blue). Scale bars: 25 μm; (c) Relative fluorescent intensities of cytoskeletal filaments in MCF 10A and MDA-MB231cell lines.

Table 1
Viscoelastic parameters of human cell's cytoskeleton used for simulations. Carmichael et al. (2015).

Cell line	E_1, (kPa)	E_2, (kPa)	η,(kPa s)
MCF 10A	170.2 ± 67.15	149.1 ± 68.46	611.34
MDA-MB-231	98.54 ± 63.63	69.12 ± 48.03	379.57

2009). $G_R(t \to \infty)$ and K_R $(t \to \infty)$ are simply expressed in terms of the long-term elastic (Young's) modulus in this paper. This is done using standard isotropic linear elastic relationships that link E and ν to the shear modulus, G, and the bulk modulus, K. The mechanical properties used are presented in Table 1.

3.4. Interfacial fracture mechanics model

The interfacial cracks between the cell membrane and the ECM or the ECM and the substrate were modeled using interfacial fracture mechanics concepts developed originally for dissimilar isotropic elastic materials, with different elastic moduli and Poisson's ratios (Teng et al., 2012; Zustiak, Nossal, and Sackett, 2014; Lei, Lawrence, and Dong, 1999; Liu and Wang, 2004; Perez, 2004). In computing the stress intensity factors, we considered the cell membrane and the ECM of the cell adhesion to be two dissimilar bi-materials with an initial opening at the cell-ECM interface (Fig. 1d). The stress field for crack lying at the interface between two dissimilar materials depends on the two Dunders' (Dunders, 1969) mismatch parameters, α and β. These are given by:

$$\alpha = \frac{\mu_1(1-\nu_2) - \mu_2(1-\nu_1)}{\mu_1(1-\nu_2) + \mu_2(1-\nu_1)} \tag{12a}$$

and

$$\beta = \frac{\frac{1}{2}\mu_1(1-2\nu_2) - \mu_2(1-2\nu_1)}{\mu_1(1-\nu_2) + \mu_2(1-\nu_1)} \tag{12b}$$

where μ is the shear modulus and ν Poisson's ratio. The subscripts 1 and 2 refer to the cell membrane and extracellular matrix, respectively. The parameters α and β are zero when the two materials have the same mechanical properties. The differences between the mechanical properties of two related materials results in axial and shear stresses along the interface. The stresses along the cell-ECM interface, near end of the interfacial membrane opening (interfacial crack tip), are given by Rice and Sih (1965) to be:

$$\sigma_y + i\tau_{xy} = \frac{Kr^{iz}}{\sqrt{2\pi r}} \tag{13}$$

where K is the complex stress intensity factor, defined by: $K = K_I + iK_{II}$, and $K_I and K_{II}$ are the components of the complex stress intensity factor. The mode mixity associated with $K_I and K_{II}$ is given by:

$$\psi = tan^{-1}\left(\frac{K_{II}}{K_I}\right) \tag{14}$$

The energy release rate for extension of a crack along the bi-material interface for a plane strain is related to the stress intensity factors via the following expression (Evans et al., 1990):

$$G = \frac{\frac{1}{E_1} + \frac{1}{E_2}}{2cosh^2(\pi\varepsilon)}(K_I^2 + K_{II}^2) \tag{15}$$

where ε is a function of material constants which depends on β(Dunders' mismatch parameter), E is the Young modulus, (1 and 2 denote the material).

In an effort to understand the deformation and detachment of single adhered cancer cells and normal cells from the uncoated surfaces, a two-dimensional model was developed. The model, which is shown schematically in Fig. 1, considered the shear assay flow chamber as a micro-channel bounded by two ridge parallel plates with viscous incompressible fluid that is driven by the applied pressure difference at the ends of the channel. The model also incorporated the initial morphologies of undeformed/detached MCF 10A and MDA-MB 231 cells obtained from 3D confocal microscopy images observed. The maximum cell height was also extracted from the confocal microscopy images. Adhesion was assumed to occur between the cell membrane and the ECM, or between the ECM and the substrate material (PDMS).

Cell/surface adhesion was treated as an interaction of discrete viscoelastic and elastic layers. For simplicity, the microvilli on the surfaces of both cancer cell and normal cell were neglected. Hence, a smooth membrane surface was assumed. Furthermore, before fluid impact on the cell, it was assumed that depolarization of actin-filament occurred was along at the frontal area of the cell membrane. This was attributed to the effects of mechano-transduction.

The induced pre-stress was also assumed to induce the interfacial opening of the cell membrane from the extracellular matrix at the contact area. The initial interfacial opening between the cell membrane and the extracellular matrix interface was treated as a fracture mechanics problem (Fig. 1d) (Perez, 2004). The finite element method (Rao, 1989; Dassault Systèmes, 2014) was then used to solve the two-dimensional fracture mechanics problem of a cell detaching from PDMS substrate. The models were used to compute the J integrals and critical stress intensity factors associated with cell detachment from the PDMS substrate.

3.5. FEM model implementation

A linear elastic fracture mechanics model was developed and used to study the detachment of single biological cells from flat substrates. The cell detachment from the PDMS substrate was modeled as an interfacial fracture problem. A two-dimensional plane model of a cell on a substrate (Fig. 1f) was developed using the ABAQUS™ software package (ABAQUS, Simulia, Pawtucket, Rhode Island, USA). The finite element model utilized 8-node, bi-quadratic, plane strain, quadrilateral elements (CPE8). This was used to discretize the two-dimensional geometry of the cell membrane/nucleus, extracellular matrix layer, and the substrates.

An approximate element size of 0.062 μm was used in the modeling. However, the cell's curved shape was modeled with curvature control with maximum deviation factor and minimum size factor (as a fraction of element size) of 0.1 μm. This was done to improve the approximations. The meshed cell-PDMS geometry consisted of an average of 5706 elements. The crack tips modeled with the triangular quarter-point elements (collapsed 8-node quadrilateral elements) (Barsoum, 1977; Saouma and Schwemmer, 1984). Path independent contour integrals were used at the cell-ECM interface to model the interfacial fracture. The models also used prior measurements of cells (Fu et al., 2009), ECM (Soucy et al., 2011) and the PDMS substrate (Park et al., 2010) to estimate the mechanical properties. These are summarized in Table 1.

The models also considered the differences between the mechanical properties of cancer cells and normal cells (Carmichael et al., 2015). These were incorporated into the finite element calculation of crack driving forces at the crack tips of different interfacial crack lengths as functions of the applied loads. The contour integral method was also used to compute the interfacial crack driving forces for the interface between the ECM layer and the substrate. The simulations of interfacial failure involved the release of nodes in the vicinity of the crack-tip, once the critical crack driving forces were reached. The time duration for the simulations was 12 min, with time steps of 0.01 s.

3.6. Statistical analysis

A paired two-sample *t*-test was conducted to determine whether the energy release rate due to the failure of cell-ECM interface varied as a function of the two types of cell line under shear loading. The statistical analyses were performed with Minitab 16 Software (Minitab Inc, Minitab 16 User Guide Manual, 2013). Since the normal breast cell and the breast cancer cells were subjected to the same shearing forces, a null hypothesis was stated and tested at 95% confidence interval for the statistical significant mean difference in energy release rate from normal breast cells and breast cancer cells detachment. The expression used to estimate the t-statistic is given by (Minitab Inc, Minitab 16 User Guide Manual, 2013):

$$t = \frac{\sum d}{\sqrt{\frac{n(\sum d^2 - (\sum d)^2)}{n-1}}} \tag{16}$$

where d is the difference between each pair of the data and n is the sample size.

4. Results and discussion

4.1. Cytoskeletal Structure

Figs. 2–4(a, b) present *confocal immunofluorescence images* of F-actin, α-tubulin, vimentin and cyto-*keratin 8 cytoskeletons* in *MCF-10A* and *MDA-MB-231 cells* associated with cell deformation and cell invasive migration. All the cells were stained and imaged under identical conditions, in which the F-actin cytoskeleton was stained red, which tubulin or vimentin or cyto-keratin 8 were stained in green, and the nucleus was stained in blue, as shown in Figs. 2–4(a, b).

To compare the cellular actin, α-tubule, vimentin and cyto-keratin 8 and filament content in MCF 10A cells and MDA-MB-231 cells, *immunofluorescence images of MCF 10A and MDA-MB-231* cell lines were analyzed using the ImageJ software (NIH, Bethesda, MD). The relative fluorescence obtained for actin/α-tubules; actin/vimentin; and actin/cyto-keratin 8 in the cell lines is presented in Fig. 4c. The result shows that the relative fluorescence intensities of the filaments are much higher in MCF 10A cells than in the MDA-MB-231 cells.

The *volume fractions of actin filaments, microtubules, vimentin and cyto-keratin 8 calculated* from 3D stacked images are presented in Table 2. The results show that the MDA-MB-231 cells expressed high vimentin concentrations and lower volume fractions of cyto-keratin 8 than the MCF 10A cells (Table 2). This *has* been *reported* in the *literature* (Agelaki et al., 2015), notably down-regulation of *cyto-keratin* and high vimentin expression in various epithelial *cancers* (Kokkinos et al., 2007; Sommers et al., 1989) and thus, significantly increases epithelial cancer cell migration, invasion and metastasis (Vuoriluoto et al., 2010; Fortier

Table 2
Estimated volume fractions of Actin, α-tubulin vimentin and cytokeratin 8 filaments in MCF 10A cell line and MDA-MB-231 cell line.

Cell line	Actin volume fraction	α-tubulin volume fraction,	Vimentin volume fraction,	Cytokeratin 8 vol fraction,
MCF 10A	0.31	0.17	0.20	0.23
MDA-MB 231	0.28	0.14	0.23	0.12

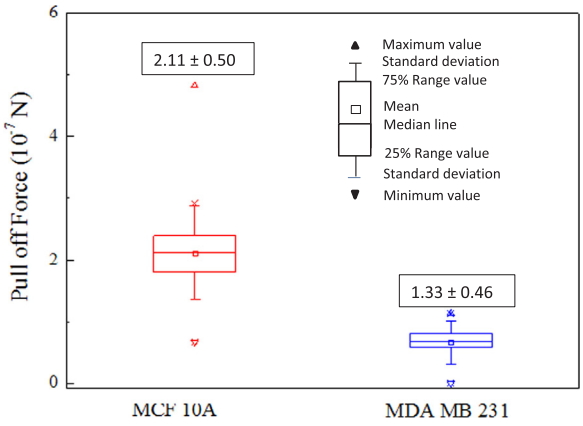

Fig. 5. Adhesion force measurement between ECM –coated AFM probes and MCF 10A/MDA-MB-231 cell lines.

et al., 2013).

4.2. AFM measurements of adhesion

The pull-off forces obtained from the AFM experiments are presented in Fig. 5. These correspond to the debond forces for the separation of the ECM from the cell membrane surfaces for normal and cancerous cells. The measured pull-off forces obtained for cancer cells were 211 ± 50nN for MCF 10A normal breast cells, 133 ± 46nN for MDA-MB-231 breast cancer cells. The current results, therefore, suggest that the adhesion forces obtained for breast cancer cells were less than those of normal breast cells.

4.3. Cell deformation

Fig. 6 shows the predictions of cell deformation that were obtained using the fluid-solid interaction technique that was used to model the shear assay experiments (Fu et al., 2009). Fig. 6a and b show resultant displacement of two selected points, SP1(100 μm, 38 μm) and SP1(126 μm, 20 μm) in the non-nuclei domain in the FEM models of the cytoplasm of MCF 10A cells and MDA-MB 231 cells (with cell height, 2.84 μm). These were subjected to different inlet fluid flow velocities into the microchannel. Note the top surface of the cell body experiences higher velocity field impact as the fluid flow over it. Hence, SP_1 is displaced more than SP_2 in cytoplasm of the two cell lines. The results presented in Fig. 6a and b show that breast cancer cells (MDA-MB-231 cells) deform more significantly than the healthy breast cells (MCF 10A cells) under the same shear flow conditions.

The stress and strain distributions associated with the detachment of cancer cells are compared with those of normal breast cells in Figs. 7(a-d) and 8(a-d). Fig. 7(a-d) show the maximum principal stress and strain distributions obtained from a cell with cell height of 2.6μm and an interfacial crack length of 0.08μm between the cell membrane and the ECM. The weaker interface between the ECM and the cell membrane fails first, with the ECM of the cancer cells experiencing lower stresses than the normal cells (Fig. 7(a-b)).

The strains in the nucleus of the cancer cell are also much greater than those of the normal breast cell. The strain distributions associated with the different stages of interface failure are presented in Fig. 8. It is

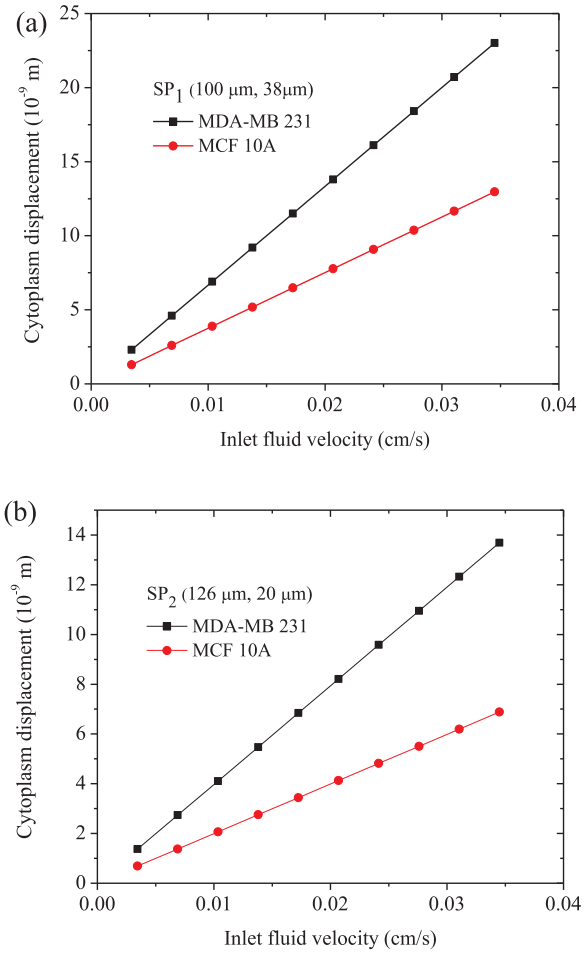

Fig. 6. Total displacement of selected points ($SP_{i=1,2}$): (a) SP_1 (100 μm, 38 μm); (b) SP_2 ($126\ \mu m$, $20\ \mu m$) in Cytoplasm of Normal cell and Cancer cell FEM model under Shear flow.

particularly interesting to note that the cell detachment process involves the bending of the cell membrane over the attached regions. Hence, during cell detachment, the bending of the cell membrane induces high compressive and tensile strains across the cell membranes.

The relatively high moduli of the nuclei also result in lower principal strains. The higher volumes fractions of cyto-keratin and actin filaments in the cytoplasm of the normal cell makes it stiffer, thus less deformable than the cytoplasm of breast cancer cell with lower volume fractions of cyto-keratin and actin filaments under the same loading conditions. Furthermore, the viscoelastic parameters of breast cancer's cytoskeleton (Table 1) and ECM layers result in higher strains in the deformed cancer cells, compared to those in the deformed normal cells.

The results of the immunofluorescence staining of vinculin, fibronectin, and laminin have been reported by Fu et al. (2009) in prior work by our research group. These were obtained immediately after the shearing process. They were used to identify the interfaces at which failure occurred (Fu et al., 2009). The vinculin stains revealed the detachment of HOS cells from the ECM. They were related to the shear-off forces at the interfaces between the cell membranes and the vinculin transmembrane proteins. This leaves behind a residue of vinculin in the

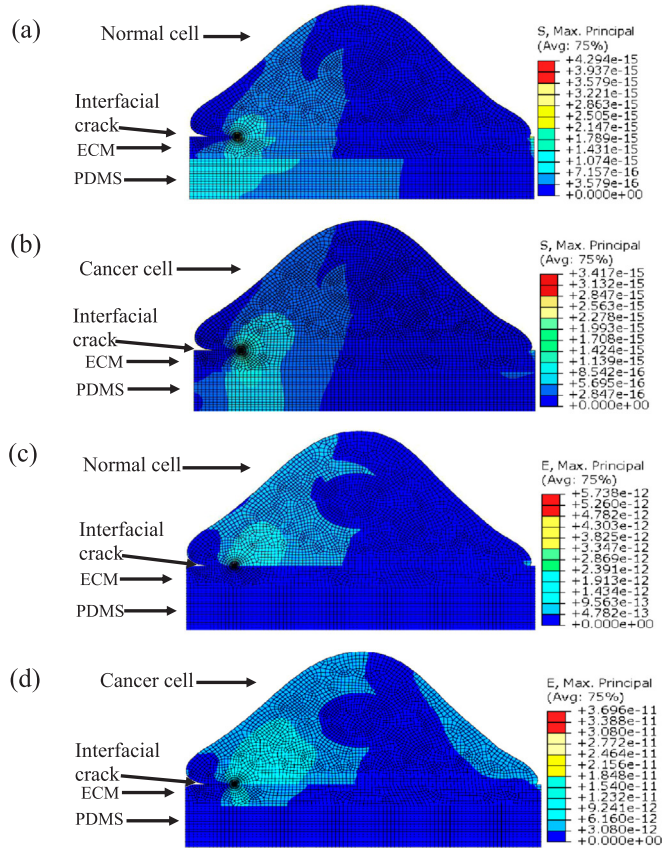

Fig. 7. Stress and Strain Distributions during Detachment of Cell-ECM with Interface Interfacial Membrane Opening of 0.08 μm: (a, c) MCF 10A Cells and (b, d) MDA-MB-231 Cells.

ECM structures that are left attached to the substrate, following the detachment of the cells during the shear assay experiments.

In the current work, similar staining protocols were also used to study the ECM structures that were left behind on the PDMS substrates after the shear assay detachment of the MCF 10A and MDA-MB-231 cells. In both cases, the staining protocols revealed a high incidence of actin and vinculin (Fig. 9a and b) on the ECM structures that were left behind on the PDMS substrates, following the detachment of the MCF 10A and MDA-MB-231 cells.

It is important to note here that the fluid shear flow gradually initiates a cell detachment process (interfacial crack) that subjects the transmembrane vinculin focal adhesion structures (FAs) to pull-out processes until they snap at the vinculin/actin interface or in the actin filaments close to the vinculin/actin interface. This leaves behind vinculin in the ECM, following the detachment of the MCF 10A cell line from the ECM, and a combination of actin terminated vinculin, following the detachment of the MDA-MB-231 cell from the ECM.

Hence, following Fig. 9a shows that lesser vinculin are involved in the focal adhesion sites (FAs) in MCF 10A cells than the MDA-MB-231 cells. As the tension continues to build-up during the pull-out of the vinculin, the resulting tractions cause the fracture of the actin filaments in regions close to the actin/vinculin interface (indicated by the white arrows). This leaves behind a distribution of vinculin co-localized with actin filaments in the residual ECM structures on the substrates (Fig. 9a and b).

Fig. 9c shows that the MCF 10A had high concentration of co-localized actin and vinculin (HC-AV) at the center of focal adhesion contact area made with the substrate, while the MDA-MB-231 cell had more localization of actin/vinculin at the cell periphery (PC-AV), as shown in Fig. 9d. This may explain why the MCF-10A (normal breast cells) were more strongly adherent and ten times stiffer than the MDA MB 231 cells (breast cancer cells) (Hu et al., 2018). Hence, the energy release rates presented in this study correspond to those required for the detachment of the cell membranes from ECM and the pull-out of the transmembrane protein structures until they snap at the vinculin/protein interface or in the actin cytoskeletal structure in a region close to the vinculin/actin interface.

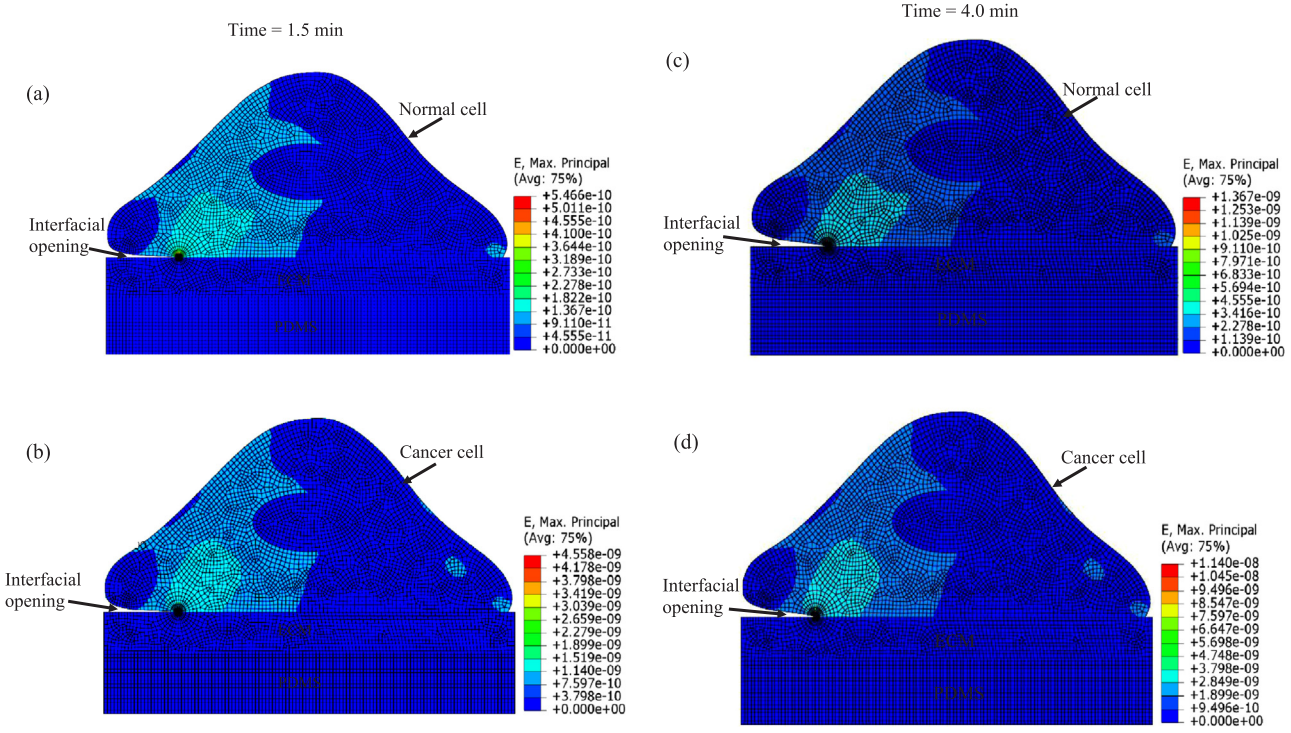

Fig. 8. Detachment of Cell-ECM Interfaces with Interfacial Membrane Opening of 0.12 μm: (a, c) MCF 10A Cells and (b, d) MDA-MB-231 Cells.

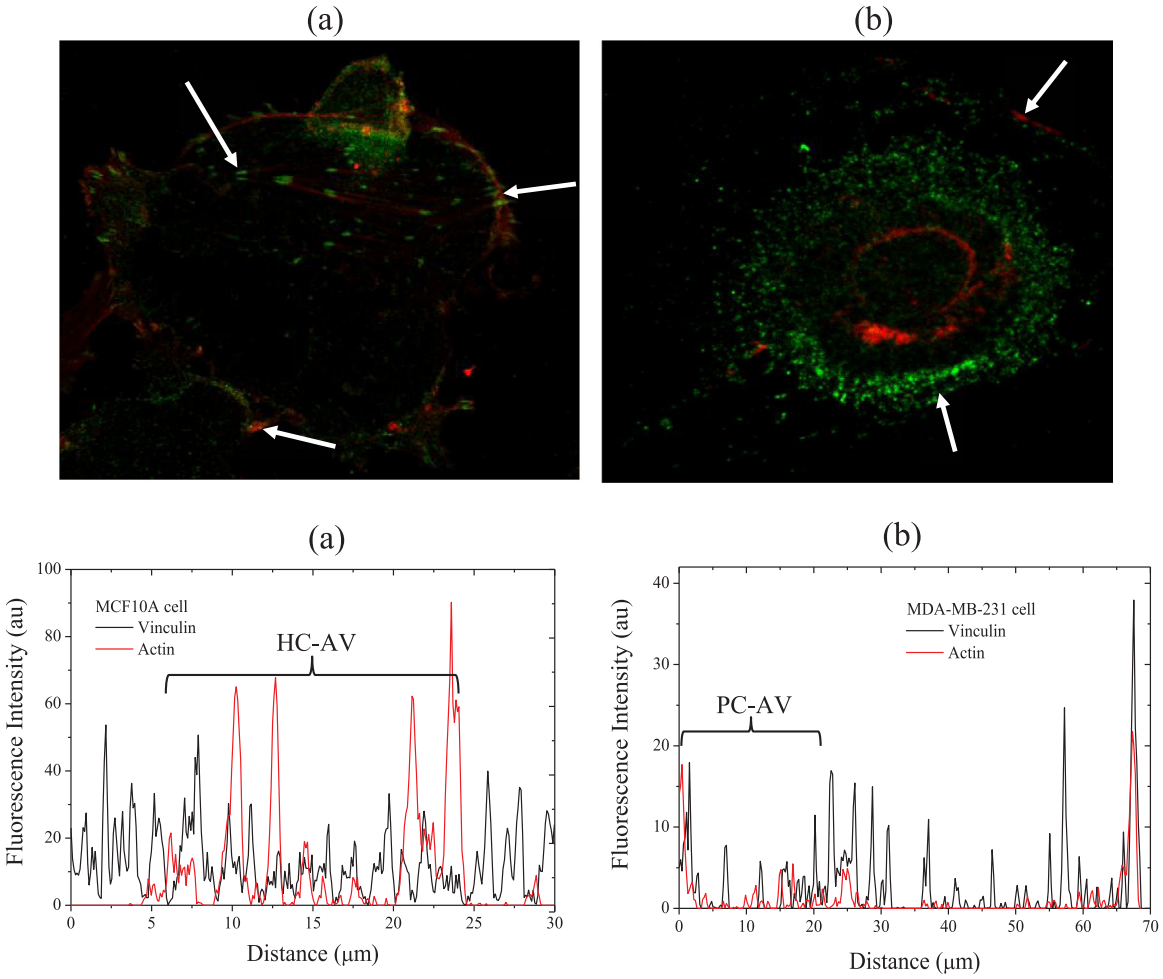

Fig. 9. Immunofluorescence staining of the Vinculin (Green) and Actin (Red) structures left on ECM after shearing off: (a) MDA-MB-231 cell, (Scale bar 20 μm); (b) MCF10A cell, (Scale bar 20 μm) and Fluorescence Intensity profiles of Actin and Vinculin left on ECM after shearing: (c) MCF 10A cell and (d) MDA-MB-231 cell.

4.4. Crack driving forces

The energy release rates associated with the detachment of normal breast cells and the breast cancer cells from ECM on the PDMS surfaces are presented in Fig. 10 for different interfacial crack lengths. The crack driving forces obtained for the normal MCF-10A breast cells were generally greater than those obtained for the MDA-MB-231 breast cancer cells, as shown in Fig. 10. The results show that lower shear forces are required to detach cancer cells than healthy normal cells with the same cell heights and interfacial crack lengths. Decreasing cell heights also result in higher cell detachment forces for both the breast cancer cells and the healthy breast cells. It is important to note that several studies have shown that the reorganization of the cytoskeletal structure that occurs during cell spreading increases the cell stiffness (Thoumine, Cardoso, and Meister, 1999; Seltmann et al., 2013; Xiong et al., 2010). Hence, such reorganization alone cannot explain the observed differences between the cytoskeletal structures of the normal and breast cancer cells.

Furthermore, the statistical test results revealed that the p values of energy release rates for each crack length are 0.283; 0.346; 0.377; 0.252; 0.565, respectively. Each of the (p-value) value is far greater than the significance level, α of 0.05. The box plot graphs also indicate that the null hypotheses (test mean) were within the 95% confidence interval of the sample mean ($\bar{x}$). This shows that the mean differences between the two cell lines are not statistically significant. The results (probability values, t-statistics and the boxplots) suggest that we fail to reject that there are significant difference in the energy release rates of the normal breast cells and the breast cancer cells under the same shear loading conditions. Hence, significant differences ($p < 0.05$) were observed between the energy release rates at the various stages of interfacial crack opening.

Similar trends were also observed for the crack driving forces of the interfacial cracks between the ECM and the PDMS substrate. However, this will not be discussed in detail, since the fluorescence microscopy revealed that the applied crack driving forces were well below the critical energy release rates required for interfacial failure (Fu et al., 2009). Hence, interfacial failure is more likely to occur between the cell membrane and the ECM than between the ECM and the substrate. This is consistent with prior experimental results reported by Cao et al., (Cao et al., 2007).

Fig. 11 shows the mode mixities associated with cell membrane-ECM interface opening for different crack lengths. The trends are quite similar for both normal breast cells and breast cancer cells. Thus, the decrease in cell height for each crack length affects the stress intensity factors ($K_I and K_{II}$) evaluated at the crack tips. The computed mode mixities decrease from the first crack length of 0.04 μm to the fourth crack length of 0.14 μm. However, the mode mixities later increase in value, for crack length of 0.2 μm. The mode mixity rise after 0.14 μm is due to the contribution of the K_{II} which is approximately 2.3 times lower than K_I.

Before closing, it is important to note that crack path selection criteria (for interfacial cracks) generally depend on the energy release rates and the mode mixity values (Fig. 11) (Hutchinson and Suo, 1991; Evans et al., 1990). Hence, the critical conditions for interfacial failure

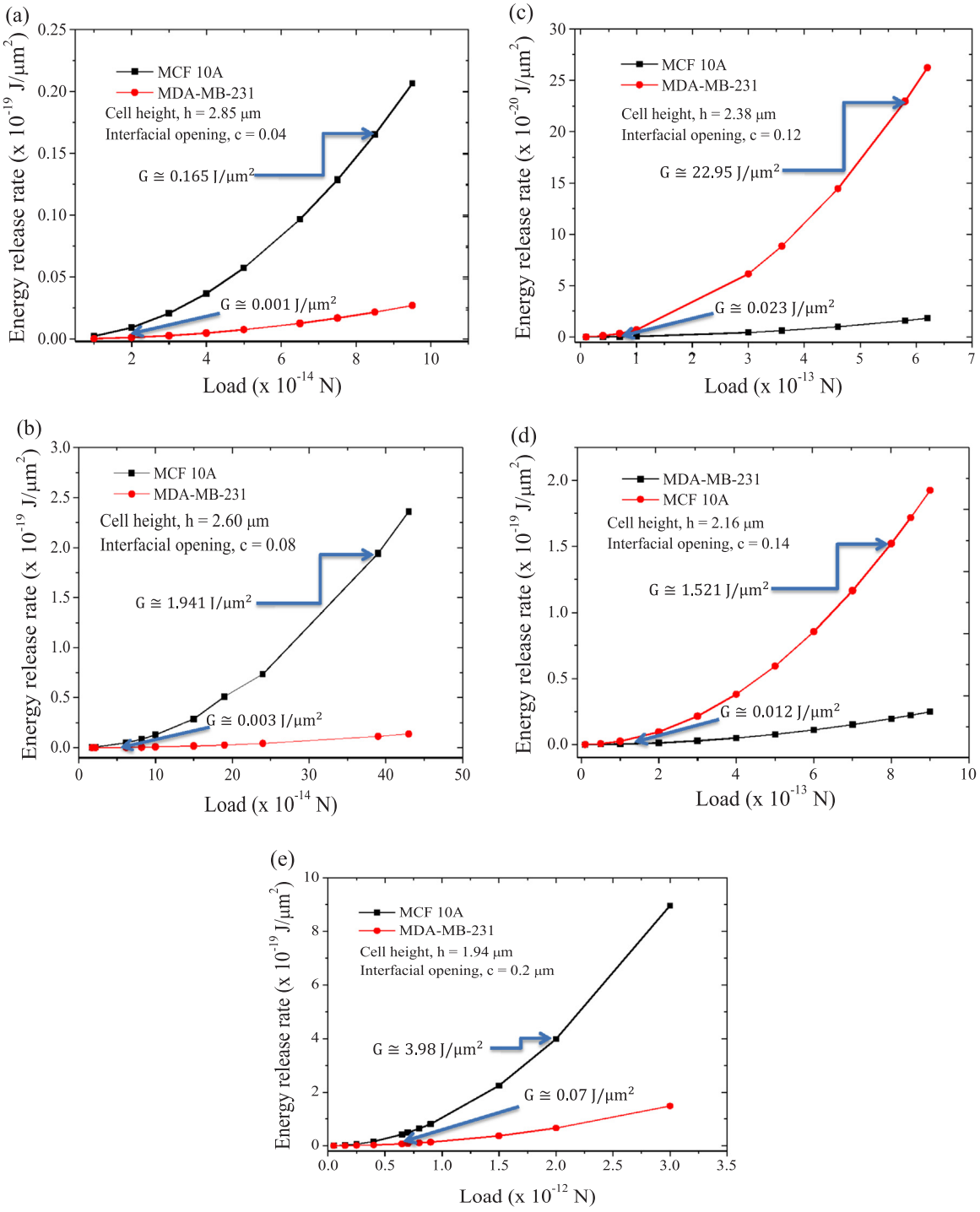

Fig. 10. Energy Release Rates For Detaching MCF 10A Cells and MDA-MB-231 Cells with Cell Height and Interfacial Opening: (a) h = 2.85 μm, c = 0.04 μm; (b) h = 2.60 μm, c = 0.08 μm; (c) h = 2.38 μm, c = 0.12 μm; (d) h = 2.16 μm, c = 0.14 μm; (d) h = 1.94 μm, c = 0.2 μm.

between the ECM and the substrate should depend on the mode mixity and energy release rates. Since the crack driving forces between the cell membrane and the ECM (Fig. 6) are much greater than those between the ECM and the PDMS substrate, the current work suggests that interfacial failure should occur first between the cell membrane and the ECM, or between the cell membrane and the vinculin transmembrane structures. This leaves behind a distribution of vinculin and patches of ECM on the PDMS substrate, following the detachement of cells from the ECM, during the fluid-induced shearing and deformation processes.

5. Implications

The implications of the current work are very significant. First, they show clearly that the cell detachment forces that occur during the shear assay experiments can be idealized as an interfacial fracture process that involves the detachment of the ECM from the cell membrane, as well as the pull-out of the vinculin transmembrane proteins from the cell. The leaves behind a significant distribution of vinculin in the residual ECM that is left behind on the PDMS substrate, following the cell detachment process (Fig. 9a and b).

Hence the detachment of the cells is associated with interfacial

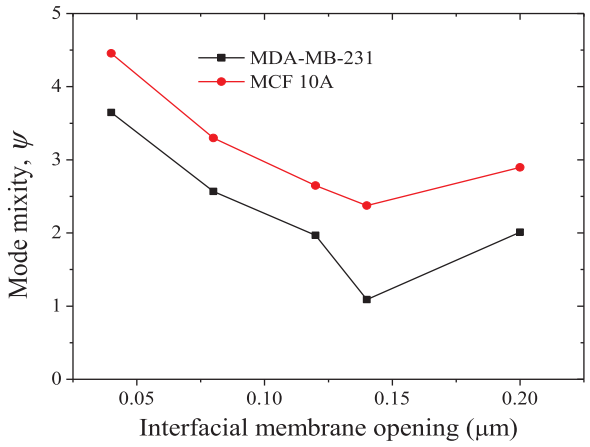

Fig. 11. Mode Mixities Obtained For Detaching Adhered MCF 10A Cells and MDA MB-231 Cells With Varying Cell Heights.

cracking between the cell membrane and the ECM, with a high incidence of crack-tip shielding by the pull-out of vinculin. The adhesion of the MCF 10A and MDA-MB-231 cells to the PDMS substrates should, therefore, depend strongly on cell membrane/ECM interactions and vinculin/cell membrane interactions. Hence, the critical crack driving forces for cell detachment (during the shear assay process) are associated with the driving forces that are needed to overcome Van der Waals forces or hydrogen bonds (secondary bonds) associated with the interactions between the ECM and the cell membrane, and vinculin transmembrane proteins and the cell membrane.

The above results suggest that the engineering of interfaces between biomedical implants and cells/tissue may be accomplished by the introduction of the constituents of ECM structures that contribute to cell adhesion. These include adhesive proteins, such as fibronectin and Arginine Glycine Aspartate (RGD) that have shown to significantly enhance the adhesion between biological cells and biomedical surfaces (Milburn et al., 2009; Bly et al., 2007; Fu et al., 2009). Such proteins can be patterned onto the surfaces of biomedical surfaces to increase the adhesion between biological cells and surfaces during the initial stages of implant integration. These are clearly some of the challenges and opportunities for future work.

6. Conclusions

The paper presents the results of a combined experimental, analytical and computational study of the shear assay detachment of normal breast cells and breast cancer cells from PDMS substrates that are relevant to biomedical implants. The cell detachment process is modeled as an interfacial cracking process. The resulting crack driving forces are also computed along with the underlying mode mixity values for interfaces between the cell membrane and the ECM, and the interfaces between the ECM and the substrate. The simulations of cell deformation and detachment reveal that breast cancer cells deform much more than normal breast cells under the same fluid flow conditions. The interfacial crack driving forces also increase with increasing shear stress and duration, resulting ultimately in interfacial failure (between the ECM and the cell membrane) when critical conditions are reached. The predictions from the simulations are consistent with experimental observations of the shear assay detachment of the cell membrane from the ECM, and the pull-out of transmembrane vinculin proteins from the cell membrane. Hence, the cell detachment process may be idealized as an interfacial fracture process (between the ECM and the cell membrane), with a high incidence of vinculin transmembrane protein bridging and pull-out.

Acknowledgments

The research was supported by the World Bank Step-B Program, The World Bank African Centers of Excellence Program, The African Development Bank, the African Capacity Building Foundation and the Nelson Mandela Institution, the Pan-African Materials Institute (PAMI) (Grant No. P126974) at the African University of Science and Technology, Abuja, Nigeria and the Worcester Polytechnic Institute (WPI). The authors are grateful the these organizations for their support.

References

Agelaki, Sofia, Chiotaki, Rena, Politaki, Eleni, Mavroudis, Dimitris, Matikas, Alexios, Georgoulias, Vassilis, Theodoropoulos, Panayiotis A., 2015. Variable expression levels of Keratin and Vimentin REveal Differential EMT status of circulating tumor cells and correlation with clinical characteristics and outcome of patients with metastatic breast cancer. BMC Cancer 15, 399–409. https://doi.org/10.1186/s12885-015-1386-7.

Barreto, Sara, Clausen, Casper H., Perrault, Cecile M., Fletcher, Daniel A., Lacroix, Damien, 2013. A multi-structural single cell model of force-induced interactions of cytoskeletal components. Biomaterials 34 (26), 6119–6126.

Barsoum, Roshdy S., 1977. Triangular quarter-point elements as elastic and perfectly-plastic crack tip elements. Int. J. Numer. Methods Eng. 11, 85–98.

Bhushan, Bharat, 1999. *Handbook of Micro/Nano Tribology*, 2nd,. *Handbook of Micro/Nano Tribology* 1,. CRC press, New York, pp. 1–737.

Bashir, Rashid, 2004. BioMEMS: state-of-the-art in detection, opportunities and prospects. Adv. Drug Deliv. Rev. 56 (11), 1565–1586. https://doi.org/10.1016/j.addr.2004.03.002.

Bly, R.A., Cao, Y., Moore, W.A., Soboyejo, W.O., 2007. Investigation of the effects of alkane Phosphonic acid/RGD coatings on cell spreading and the interfacial strength between human osteosarcoma cells and Ti–6Al–4V. Mater. Sci. Eng.: C 27 (1), 83–89.

Cailleau, R., Young, R., Olive, M., Reeves, W.J., 1974. Breast tumor cell lines from pleural effusions. J. Natl. Cancer Inst. 53 (3), 661–674.

Cao, Yifang, Bly, Randy, Moore, Will, Gao, Zhan, Cuitino, Alberto M., Soboyejo, Wole, 2007. On the measurement of human osteosarcoma cell elastic modulus using shear assay experiments. J. Mater. Sci.: Mater. Med. 18 (1), 103–109.

Carmichael, B., Babahosseini, H., Mahmoodi, S.N., Agah, M., 2015. The Fractional Viscoelastic Response of Human Breast Tissue Cells. Physical Biology 12. IOP Publishing, pp. 46001. https://doi.org/10.1088/1478-3975/12/4/046001.

Cary, Robert B., Klymkowsky, Michael W., Evans, Robert M., Domingo, Alberto, Dent, Joseph A., Backhus, Leilah E., 1994. Vimentin's tail interacts with actin-containing structures in vivo. J. Cell Sci. 107, 1609–1622.

Croop, J., Holtzer, H., 1975. Response of myogenic and fibrogenic cells to Cytochalasin B And to Colcemid I. J. Cell Biol. 65, 271–285.

Cross, Sarah E., Jin, Yu-Sheng, Rao, Jianyu, Gimzewski, James K., 2007. Nanomechanical analysis of cells from cancer patients. Nat. Nanotechnol. 2 (12) (780–763).

Curtis, Matthew W., Russell, Brenda, 2009. Cardiac tissue engineering. J. Cardiovasc. Nurs. 24 (2), 87–92.

Dassault Systèmes, 2014. Abaqus 6.12/CAE. User's Manual, Pawtucket. Rode Island, USA.

Dong, Cheng, Cao, Jian, Struble, Erika J., Lipowsky, Herbert H., 1999. Mechanics of leukocyte deformation and adhesion to endothelium in shear flow. Ann. Biomed. Eng. 27 (3), 298–312.

Dong, Cheng, Lei, Xiao X., 2000. Biomechanics of cell rolling: shear flow, cell-surface adhesion, and cell deformability. J. Biomech. 33 (1), 35–43.

Dunders, J., 1969. Edge bonded dissimilar orthogonal elastic wedges under normal and shear loading. J. Appl. Mech. 36, 650–652.

Efremov, Yu. M., Dokrunova, A.A., Efremenko, A.V., Kirpichnikov, M.P., Shaitan, K.V., Sokolova, O.S., 2015. Distinct impact of targeted actin cytoskeleton reorganization on mechanical properties of normal and malignant cells. BBA - Mol. Cell Res. 3117–3125. https://doi.org/10.1016/j.bbamcr.2015.05.008.

Engler, Adam J., Chan, May, Boettiger, David, Schwarzbauer, Jean E., 2009. A novel mode of cell detachment from Fibrillar Fibronectin matrix under shear. J. Cell Sci. 122, 1647–1653. https://doi.org/10.1242/jcs.040824.

Erler, Janine T., Bennewith, Kevin L., Nicolau, Monica, Dornhöfer, Nadja, Kong, Christina, Le, Quynh-Thu, Ashley Chi, Jen-Tsan, Jeffrey, Stefanie S., Giaccia, Amato J., 2006. Lysyl oxidase is essential for hypoxia-induced metastasis. Nature 440 (7088), 1222–1226.

Esue, Osigwe, Carson, Ashley A., Tseng, Yiider, Wirtz, Denis, 2006. A direct interaction between actin and vimentin filaments mediated by the tail domain of vimentin. J. Biol. Chem. 281 (41), 30393–30399. https://doi.org/10.1074/jbc.M605452200.

Evans, A.G., Rühle, M., Dalgleish, B.J., Charalambides, P.G., 1990. The fracture energy of bimaterial interfaces. Metall. Trans. 21 (9), 2419–2429.

Evans, Evan A., 1980. Minimum energy analysis of membrane deformation applied to pipet aspiration and surface adhesion of red blood cells. Biophys. J. 30 (2), 265–284.

Fallqvist, Bjorn, Matthew, L. Fielden, Pettersson, Torbjorn, Nordgren, Niklas, Kroon, Martin, Gad, Annica K.B., 2016. Experimental and computational assessment of F-Actin influence in regulating cellular stiffness and relaxation behaviour of fibroblasts. J. Mech. Behav. Biomed. Mater. 59, 168–184. https://doi.org/10.1016/j.jmbbm.2015.11.039.

Fisseha, Demeke, Katiyar, V.K., 2012. Analysis of mechanical behavior of red cell membrane in sickle cell disease. Appl. Math. 2 (2), 40–46.

Fletcher, Daniel A., Mullins, R. Dyche, 2010. Cell mechanics and the cytoskeleton. Nature 463 (7280), 485–492.
Fortier, Anne-marie, Asselin, Eric, Cadrin, Monique, Fortier, Anne-marie, Asselin, Eric, Cadrin, Monique, 2013. Keratin 8 and 18 Loss in Epithelial Cancer Cells Increases Collective Cell Migration and Cisplatin Sensitivity through. https://doi.org/10.1074/jbc.M112.428920.
Fu, G., Milburn, C., Mwenifumbo, S., Cao, Y., Oparinde, G.M., Adeoye, M.O., Therialt, C., Beye, A.C., Soboyejo, W.O., 2009. Shear assay measurements of cell adhesion on biomaterials surfaces. Mater. Sci. Eng.: C 29 (4), 1293–1301.
Fuhrmann, A., Staunton, J.R., Nandakumar, V., Banyai, N., Davies, P.C.W., Ros, R., 2011. AFM stiffness nanotomography of normal, Metaplastic and dysplastic human esophageal cells. Phys. Biol. 8 (1), 15007.
Gaver, Donald P., Kute, Stephanie M., 1998. A theoretical model study of the influence of fluid stresses on a cell adhering to a microchannel wall. Biophysical 75 (2), 721–733.
Gavet, Olivier, Pines, Jonathon, 2010. Progressive activation of cyclinb1-cdk1 coordinates entry to Mitosis. Dev. Cell 533–543. https://doi.org/10.1016/j.devcel.2010.02.013.
Gibson, Ronald F., 1994. Principles of Composite Material Mechanics, 3rd ed. McGraw-Hill, Inc, New York.
Gladilina, Evgeny, Gonzaleza, Paula, Eilsa, Roland, 2014. Dissecting the Contribution of Actin and Vimentin Intermediate Filaments to Mechanical Phenotype of Suspended Cells Using High-Throughput Deformability Measurements and Computational Modeling. pp. 2598–2605.
Goldman, Robert D., Satya Khuon, Ying Hao, Chou, Puneet, Opal, Steinert, Peter M., 1996. The function of intermediate filaments in cell shape and cytoskeletal integrity. J. Cell Biol. 134 (4), 971–983.
Green, Kathleen J., Goldman, Robert D., 1983. The effects of taxol on cytoskeletal components in cultured fibroblasts and epithelial cells. Cell Motil. 3 (4), 283–305.
Guo, Qiuquan, Xia, Ying, Sandig, Martin, Yang, Jun, 2012. Characterization of cell elasticity correlated with cell morphology by atomic force microscope. J. Biomech. 45 (2), 304–309.
Hampp, E., Botah, R., Odusanya, O.S., Anuku, N., Malatesta, K.A., Soboyejo, W.O., 2012. Biosynthesis and adhesion of gold nanoparticles for breast cancer detection and treatment. J. Mater. Res. 27 (22), 2891–2901.
Hong-Lian, G.U.O., Chun-Xiang, L.I.U., Jian-Fa, D.U.A.N., Yu-Qiang, J.I.A.N.G., Xue-Hai, H.A.N., Zhao-Lin, L.I., Bing-Ying, C.H.E.N.G., Dao-Zhong, Z.H.A.N.G., 2004. Mechanical properties of breast cancer cell membrane studied with optical tweezers. Chin. Phys. Lett. 21 (12), 2543–2546.
Hu, Jingjie, Zhou, Yuxiao, Obayemi, John D., Du, Jing, Soboyejo, Winston O., 2018. An investigation of the viscoelastic properties and the actin cytoskeletal structure of triple negative breast cancer cells. J. Mech. Behav. Biomed. Mater. https://doi.org/10.1016/j.jmbbm.2018.05.038.
Hult, J., Rammerstorfer, F.G. (Eds.), 1994. Engineering Mechanics of Fibre Reinforced Polymers and Composite Structures. Springer-Verlag Wien, New York.
Hutchinson, John W., Suo, Zhigang, 1991. Mixed mode cracking in layered materials. Adv. Appl. Mech. 29, 63–191.
Hutter, Jeffrey L., Bechhoefer, John, 1993. Calibration of atomic-force microscope tips. Rev. Sci. Instrum. 64 (7), 1868–1873.
Hynes, R.O., 2002. Integrins: bidirectional, allosteric signaling machines. Cell 110, 673–687.
Isermann, Philipp, Lammerding, Jan, 2013. Nuclear mechanics and mechanotransduction in health and disease. Curr. Biol. 23 (24), R1113–R1121.
Iversen, Kine, 2015. Biological Cell Models and Atomic Force Microscopy: A Literature Review. Norwegian University of Science and Technology.
Izzard, C.S., Lochner, L.R., 1976. Cell-to-substrate contacts in living fibroblasts: an interference reflexion study with an evaluation of the technique. J. Cell Sci. 21, 129–159.
Janmaleki, M., Pachenari, M., Seyedpour, S.M., Shahghadami, R., Sanati-Nezhad, A., 2016. Impact of Simulated Microgravity on Cytoskeleton and Viscoelastic Properties of Endothelial Cell. Sci. Rep. 6, 32418. https://doi.org/10.1038/srep32418.
Katz, Joseph, 2010. Introductory Fluid Mechanics. Cambridge University Press, New York.
Kokkinos, Maria I., Razan Wafai, Meng Kang, Wong, Donald F., Newgreen, Erik W., Thompson, Waltham, Mark, 2007. Vimentin and epithelial-mesenchymal transition in human breast cancer – observations in vitro and in vivo. Cells Tissues Organs 185, 191–203. https://doi.org/10.1159/000101320.
Korb, Timo, Schlu, Kerstin, Enns, Andreas, Spiegel, Hans-ulrich, Senninger, Norbert, Nicolson, Garth L., Haier, Jorg, 2004. Integrity of actin fibers and microtubules influences metastatic tumor cell adhesion. Exp. Cell Res. 299, 236–247. https://doi.org/10.1016/j.yexcr.2004.06.001.
Kubitschke, H., Schnauss, J., Nnetu, K.D., Warmt, E., Stange, R., Kaes, J., 2017. Actin and microtubule networks contribute differently to cell response for small and large strains. New J. Phys. 93003.
Kuznetsova, Tatyana G., Starodubtseva, Maria N., Yegorenkov, Nicolai I., Chizhik, Sergey A., Zhdanov, Renat I., 2007. Atomic force microscopy probing of cell elasticity. Micron 38 (8), 824–833.
Lee, G.Y.H., Lim, C.T., 2007. Biomechanics approaches to studying human diseases. Trends Biotechnol. 25, 111–118.
Lei, X., Lawrence, M.B., Dong, C., 1999. Influence of cell deformation on leukocyte rolling adhesion in shear flow. J. Biomech. Eng. 121 (6), 636–643.
Lekka, M., Laidler, P., Gil, D., Lekki, J., Stachura, Z., Hrynkiewicz, A.Z., 1999. Elasticity of normal and cancerous human bladder cells studied by scanning force microscopy. Eur. Biophys. J. 28 (4), 312–316.
Li, Qingsen, Lim, Chwee Teck, 2010. Structure–Mechanical Property Changes in Nucleus Arising from Breast Cancer. Cellular and Biomolecular Mechanics and Mechanobiology. Springer-Verlag, Berlin Heidelberg, pp. 465–475.
Liu, X.H., Wang, X., 2004. The deformation of an adherent leukocyte under steady shear flow: a numerical study. J. Biomech. 37 (7), 1079–1085.
Matei, G.A., Thoreson, E.J., Pratt, J.R., Newell, D.B., Burnham, N.A., 2006. Precision and accuracy of thermal calibration of atomic force microscopy cantilevers. Rev. Sci. Instrum. 77, 83703. https://doi.org/10.1063/1.2336115.
Maxwell, Dustin J., Hicks, Brandon C., Parsons, Sarah, Skiyama-Elbert, Shelly E., 2005. Development of rationally designed affinity-based drug delivery systems. Acta Biomater. 1 (1), 101–113.
McCormick, Mary, Beth, Panos, Kouklis, Andrew, Syder, Fuchs, Elaine, 1993. The roles of the rod end and the tail in Vimentin IF assembly and IF network formation. J. Cell Biol. 122 (2), 395–407.
McGarry, J.P., 2009. Characterization of cell mechanical properties by computational modeling of parallel plate compression. Ann. Biomed. Eng. 37 (11), 2317–2325.
Milburn, C., Chen, J., Cao, Y., Oparinde, G.M., Adeoye, M.O., Beye, A., Soboyejo, W.O., 2009. Investigation of effects of argenine – glycine – aspartate (RGD) and nano-scale titanium coatings on cell spreading and adhesion. Mater. Sci. Eng. C 306–314. https://doi.org/10.1016/j.msec.2008.07.003.
Minitab Inc., Minitab 16 User Guide Manual, 2013. Pennsylvanian, USA.
Mofrad, Mohammad R.K., Kamm, Roger D. (Eds.), 2006. Cytoskeletal Mechanics: Models and Measurements in Cell Mechanics. Cambridge University Press, Cambridge, UK.
Moy, Vincent T., Jiao, Yuekan, Hillmann, Thomas, Lehmann, Horst, Sano, Takeshi, 1999. Adhesion energy of receptor-mediated interaction measured by elastic deformation. Biophys. J. 76 (3), 1632–1638.
Nematbakhsh, Yasaman, Pang, Kuin Tian, Lim, Chwee Teck, 2017. Correlating the Viscoelasticity of Breast Cancer Cells with Their Malignancy. Convergent Science Physical Oncology 3. IOP Publishing, pp. 34003.
NIH, 2012. Bethesda, MD, USA. ImageJ User Guide.
Pachenari, M., Seyedpour, S.M., Janmaleki, M., Babazadeh Shayan, S., Taranejoo, S., Hosseinkhani, H., 2014. Mechanical properties of cancer cytoskeleton depend on actin Fi laments to microtubules content: investigating different grades of colon cancer cell lines. J. Biomech. 373–379. https://doi.org/10.1016/j.jbiomech.2013.11.020.
Park, Joong Yull, Ju Yoo, Sung, Lee, Eun-joong, Lee, Dae Ho, Kim, Ji. Young, Lee, Sanghoon, 2010. Increased Poly (Dimethylsiloxane) stiffness improves viability and morphology of mouse fibroblast cells. BioChip J. 4 (3), 230–236. https://doi.org/10.1007/s13206-010-4311-9.
Peeters, E.A.G., Oomens, C.W.J., Bouten, C.V.C., Bader, D.L., Baaijens, F.P.T., 2005. Mechanical and failure properties of single attached cells under compression. J. Biomech. 38 (8), 1685–1693.
Perez, N., 2004. Fracture Mechanics. Kluwer Academic, Boston.
Pettermann, H.E., Hüsing, J., 2012. Modeling and simulation of relaxation in viscoelastic open cell materials and structures. Int. J. Solids Struct. 2848–2853. https://doi.org/10.1016/j.ijsolstr.2012.04.027.
Prat-vidal, Cristina, Roura, Santiago, Soler-botija, Carolina, Ga, Carolina, Bayes-genis, Antoni, 2013. Cardiac tissue engineering and the bioartificial heart. Rev. Esp. Cardiol. 66 (5), 391–399.
Prechtel, K., Bausch, A.R., Marchi-Artzner, V., Kantlehner, M., Kessler, H., Merkel, R., 2002. Dynamic force spectroscopy to probe adhesion strength of living cells. Phys. Rev. Lett. 89 (2), 28101.
Ramms, Lena, Fabris, Gloria, Windoffer, Reinhard, Schwarz, Nicole, Springer, Ronald, Zhou, Chen, Lazar, Jaroslav, et al., 2013. Keratins as the main component for the mechanical integrity of Keratinocytes. Proc. Natl. Acad. Sci. USA 110 (46), 18513–18518. https://doi.org/10.1073/pnas.1313491110.
Rao, S.S., 1989. The Finite Method in Engineering, 2nd ed. Elsevier Science & Technology, Oxford.
Rice, J.R., Sih, George C., 1965. Plane problems of cracks in dissimilar media. J. Appl. Mech. 32 (2), 8936.
Rinko, Linda J., Lawrence, Michael B., Guilford, William H.J.O., 2004. The molecular mechanics of P-and L-Selectin Lectin domains binding to PSGL-1. Biophys. J. 86 (1), 544–554.
Saouma, Victor E., Schwemmer, David, 1984. Numerical evaluation of the quarter-point crack tip element. Int. J. Numer. Methods Eng. 20, 1629–1641.
Sato, M., Ohshima, N., Nerem, R.M., 1996. Viscoelastic properties of cultured porcine aortic endothelial cells exposed to shear stress. J. Biomech. 29 (4), 461–467.
Sato, M., Theret, D.P., Wheeler, L.T., Ohshima, N., Nerem, R.M., 1990. Application of the micropipette technique to the measurement of cultured porcine aortic endothelial cell viscoelastic properties. J. Biomech. Eng. 112 (3), 263–268.
Schierbaum, Nicolas, Rheinlaender, Johannes, Schäffer, Tilman E., 2017. Viscoelastic properties of normal and cancerous human breast cells are affected differently by contact to adjacent cells. Acta Biomater. 239–248. https://doi.org/10.1016/j.actbio.2017.04.006.
Seltmann, Kristin, Fritsch, Anatol W., Käs, Josef A., Magin, Thomas M., 2013. Keratins Signi Fi Cantly contribute to cell stiffness and impact invasive behavior. Proc. Natl. Acad. Sci. USA 110 (46), 18507–18512. https://doi.org/10.1073/pnas.1310493110.
Soboyejo, Wole, 2002. Mechanical Properties of Engineered Materials. Marcel Dekker, Inc, New York.
Sommers, Connie L., Walker-jones, Dorothy, Heckford, Susan E., Worland, Peter, Valverius, Eva, Clark, Robin, Mccormick, Frank, Stampfer, Martha, Abularach, Silvia, Gelmann, Edward P., 1989. Vimentin rather than keratin expression in some hormone-independent breast cancer cell lines and in oncogene-transformed mammary epithelial cells. Cancer Res. 49, 4258–4264.
Soucy, Patricia A., Werbin, Jeffery, Heinz, William, Hoh, Jan H., Romer, Lewis H., 2011. Microelastic properties of lung cell-derived extracellular matrix. Acta Biomater. 7 (1), 96–105.
Spencer, Virginia A., 2011. Actin-towards a deeper understanding of the relationship between tissue context, cellular function and tumorigenesis. Cancers 3 (4),

4269–4280. https://doi.org/10.3390/cancers3044269.
Stein, Andrew M., Vader, David A., Weitz, David A., Sander, Leonard M., 2011. The micromechanics of three dimensional collagen I gels. Complexity 16 (4), 22–28.
Suresh, Subra, 2007. Biomechanics and biophysics of cancer cells. Acta Biomater. 2, 413–438.
Suresh, Subra, Spatz, J., Mills, J.P., Micoulet, Alexandre, Dao, M., Lim, C.T., Beil, M., Seufferlein, T., 2005. Connections between single-cell biomechanics and human disease states: gastrointestinal cancer and malaria. Acta Biomater. 1 (1), 15–30.
Tan, Samuel C.W., Wen, X. Pan, Ma, Gang, Cai, Ning, Leong, Kam W., Liao, Kin, 2008. Viscoelastic behaviour of human mesenchymal stem cells. BMC Cell Biol. 9 (1), 40.
Teng, Yanqun, Qiu, Juhui, Zheng, Yiming, Luo, Xiangdong, Zhang, Linlin, Chen, Li, Wang, Guixue, 2012. Effects of Type I collagen and fibronectin on regulation of breast cancer cell biological and biomechanical characteristics. J. Med. Biol. Eng. 34 (1), 62–68.
Thoumine, O., Cardoso, O., Meister, J.J., 1999. Changes in the mechanical properties of fibroblasts during spreading: a micromanipulation study. Eur. Biophys. J. 28, 222–234.
Tözeren, Aydin, Sung, K.L., Sung, Lanping A., Dustin, Michael L., Chan, Po.Ying, Springer, Timothy A., Chien, Shu, 1992. Micromanipulation of adhesion of a Jurkat cell to a planar bilayer membrane containing lymphocyte function-associated antigen 3 molecules. J. Cell Biol. 116 (4), 997–1006.
Trickey, Wendy R., Vail, T. Parker, Guilak, Farshid, 2004. The role of the cytoskeleton in the viscoelastic properties of human articular chondrocytes. J. Orthop. Res. 22, 131–139. https://doi.org/10.1016/S0736-0266(03)00150-5.
Unnikrishnan, G.U., Unnikrishnan, V.U., Reddy, J.N., 2007. Constitutive material modeling of cell: a micromechanics approach. J. Biomech. Eng. 129 (3), 315–323. https://doi.org/10.1115/1.2720908.
Vuoriluoto, K., Haugen, H., Kiviluoto, S., Mpindi, J.-P., Nevo, J., Gjerdrum, C., Tiron, C., Lorens, J.B., Ivaska, J., 2010. Vimentin regulates EMT induction by slug and oncogenic H-Ras and migration by governing Axl expression in breast cancer. Oncogene 1436–1448. https://doi.org/10.1038/onc.2010.509.
Weber, Kari L., Bement, William M., 2002. F-actin serves as a template for cytokeratin organization in cell free extracts. J. Cell Sci. 115 (7), 1373–1382.
Weisenberg, Brian A., Mooradian, Daniel L., 2002. Hemocompatibility of materials used in Microelectromechanical systems: platelet adhesion and morphology in vitro. J. Biomed. Mater. Res. 60 (2), 283–291.
Wickstrom, Mark L., Khan, Safdar A., Haschek, Wanda M., Wyman, John F., Eriksson, John E., Schaeffer, David J., Beasley, V.A.L.R., 1995. Alterations in microtubules, intermediate filaments, and microfilaments induced by Microcystin-LR in cultured cells. Toxicol. Pathol. 23 (3), 326–337.
Williamson, J.R., Gardner, R.A., Boylan, C.W., Carroll, G.L., Chang, K., Marvel, J.S., Gonen, B., Kilo, C., Tran-Son-Tay, R., Sutera, S.P., 1985. Microrheologic investigation of erythrocyte deformability in diabetes mellitus. Blood 65 (2), 283–288.
Wolf, Kurt V., Zong, Zong, Meng, Juan, Orana, Argjenta, Rahbar, Nima, Balss, Karin M., Papandreou, George, Maryanoff, Cynthia A., Soboyejo, Wole, 2008. An investigation of adhesion in drug-eluting stent layers. J. Biomed. Mater. Res. Part A 87 (1), 272–281.
Wong, K.K.L., Li, W., An, Y., Duan, Y., Li, Z., Kang, Y., Yan, Y., 2015a. B-spectrin regulates the hippo signaling pathway and modulates the basal actin network. J. Biol. Chem. 290 (10), 6397–6407. https://doi.org/10.1074/jbc.M114.629493.
Wong, Kenneth Kin, Lam, Wenyang, Li, Yanru, An, Yangyang, Duan, Zhuoheng, Li, Yibin, Kang, Yan, Yan, 2015b. β-spectrin regulates the hippo signaling pathway and modulates the basal actin network. J. Biol. Chem. 290 (10), 6397–6407. https://doi.org/10.1074/jbc.M114.629493.
Xiao, Yao, Truskey, George A., 1996. Effect of Receptor-Ligand Affinity on the Strength of Endothelial Cell Adhesion. Biophys. J. 71 (5), 2869–2884.
Xiong, Yuguang, Rangamani, Padmini, Fardin, Marc-Antoine, Lipshtat, Azi, Dubin-Thaler, Benjamin, Rossier, Olivier, Sheetz, Michael P., Iyengar, Ravi, 2010. Mechanisms controlling cell size and shape during isotropic cell spreading. Biophys. J. 98, 2136–2146. https://doi.org/10.1016/j.bpj.2010.01.059.
Xu, Wenwei, Mezencev, Roman, Kim, Byungkyu, Wang, Lijuan, McDonald, John, Sulchek, Todd, 2012a. Cell stiffness is a biomarker of the metastatic potential of ovarian cancer cells. PLos One 7 (10), e46609.
Xu, Wenwei, Mezencev, Roman, Kim, Byungkyu, Wang, Lijuan, McDonald, John, Sulchek, Todd J.O., 2012b. Cell stiffness is a biomarker of the metastatic potential of ovarian cancer cells. PLoS One 7 (10), e46609.
Xue, Feng, Mckayed, Katey K, Campbell, Veronica A, Lennon, Alex B, Prendergast, Patrick J, 2015. Effect of membrane stiffness and cytoskeletal element density on mechanical stimuli within cells: an analysis of the consequences of ageing in cells. Comput Methods Biomech. Biomed. Eng. 18 (5), 468–476.
Yamamoto, Akiko, Mishima, Shuzo, Maruyama, Norio, Sumita, Masae, 1998. A new technique for direct measurement of the shear force necessary to detach a cell from a material. Biomaterials 19 (7–9), 871–879.
Yan, Yuling, Marriott, Gerard, 2003. Fluorescence resonance energy transfer imaging microscopy and fluorescence polarization imaging microscopy. Methods Enzymol. 360, 561–580.
Yoon, Sang-Hee, Mofrad, Mohammad R.K., 2011. Cell adhesion and detachment on gold surfaces modified with a Thiol-functionalized RGD peptide. Biomaterials 32 (30), 7286–7296.
Zhou, E.H., Lim, C.T., Quek, S.T., 2005. Finite element simulation of the micropipette aspiration of a living cell undergoing large viscoelastic deformation. Mech. Adv. Mater. Struct. 12 (6), 501–512.
Zustiak, Silviya, Nossal, Ralph, Sackett, Dan L., 2014. Multiwell stiffness assay for the study of cell responsiveness to cytotoxic drugs. Biotechnol. Bioeng. 111 (2), 396–403.
Zwerger, Monika, Ho, Chin Yee, Lammerding, Jan, 2011. Nuclear mechanics in disease. Annu. Rev. Biomed. Eng. 13, 397–428.